NASA TECHNICAL NOTE

NASA TN D-2843

NASA TN D-2843

SECOND-ORDER PERTURBATION ANGLE TECHNIQUES FOR ACCURATELY SIMULATING SIGHTING PROBLEMS OF A SPACE SEXTANT

by Richard L. Kurkowski and Kenneth C. Grover

Ames Research Center
Moffett Field, Calif.

NATIONAL AERONAUTICS AND SPACE ADMINISTRATION • WASHINGTON, D. C. • MAY 1965

NASA TN D-2843

SECOND-ORDER PERTURBATION ANGLE TECHNIQUES FOR ACCURATELY SIMULATING SIGHTING PROBLEMS OF A SPACE SEXTANT

By Richard L. Kurkowski and Kenneth C. Grover

Ames Research Center
Moffett Field, Calif.

NATIONAL AERONAUTICS AND SPACE ADMINISTRATION

For sale by the Clearinghouse for Federal Scientific and Technical Information
Springfield, Virginia 22151 – Price $3.00

SECOND-ORDER PERTURBATION ANGLE TECHNIQUES FOR ACCURATELY SIMULATING SIGHTING PROBLEMS OF A SPACE SEXTANT

By Richard L. Kurkowski and Kenneth C. Grover
Ames Research Center

SUMMARY

24382

The performance of a vehicle-mounted servo-operated space sextant has been investigated with a fixed-cockpit analog-computer simulation. Computational accuracy of 1 arcsec was obtained with second-order perturbation angle techniques on the analog computer. A detailed description of the mathematical derivation is presented. Some typical results are included. The over-all system, which incorporated a cathode ray tube display, had an accuracy level of ±2 arcsec with a man in the loop and no vehicle or target motion. The effects of target and vehicle motion were studied and indications were that for 3σ sighting accuracies of ±10 arcsec or less rates must be less than 200 arcsec/sec. Optical characteristics of the sextant were ×27 and 1.8° field of view.

AUTHOR

INTRODUCTION

The sextant has been used for many years for terrestrial navigation, primarily in the form of a hand-held device. More recently, vehicle-mounted hand-operated sextants are used as the primary navigation instrument on board large military aircraft. However, for space navigation, information on the ability of a man to use such an instrument while on board a space vehicle is obviously lacking. To minimize the amount of fuel used for velocity corrections during the space flight, the angles between celestial bodies must be measured with extreme precision (i.e., a few seconds of arc). For such accuracy a high degree of magnification is required; consequently, the field of view is small. As the relative motion of the sighting objects increases, either as a result of the vehicle's rotation or translation with respect to an object sighted, the measurement task is expected to become quite difficult. With such problems in mind, a simulator investigation was undertaken to obtain basic information on the navigator's ability to make the necessary navigational measurements with optical instruments on board the spacecraft.

The simulator consisted of a fixed cockpit, an analog computer, and a manually controlled sextant mounted in the cockpit. The effects of the size and motion of the target sighted, the vehicle motion, and other system parameters on the measurement accuracy and operation of the navigator-sextant combination were evaluated. The data from this study are contained in reference 1. The purpose of the present report is to describe the derivation of the mathematical model and the details of the simulator. The simulation

is considered unique in that a high degree of accuracy, ±2 arcsec, was obtained with a conventional analog computer and a cathode ray tube display.

NOTATION

e angular measurement error at mark, arcsec

M reticle lines perpendicular to the measurement plane of the sextant (The principal M line passes through the center of the field of view.)

n number of trials per set of sighting conditions

$\bar{N}_{pitch}$ average number of pitch controller pulses

$\bar{N}_{roll}$ average number of roll controller pulses

$\bar{N}_{yaw}$ average number of yaw controller pulses

R reticle reference line which defines the measurement plane of the sextant

t time to perform task, that is, lapsed time from "start task" to "mark," sec of time

t_{av} average time required for sighting task = $\frac{1}{n}\sum_{i=1}^{n} t_i$, sec of time

σ standard deviation, defined as the root mean square of the deviations e_i of a set of observations from the true value (known to within 1 arcsec for this simulation study),

$$\sqrt{\frac{\sum_{i=1}^{n} (e_i)^2}{n}}, \text{ arcsec}$$

Vector Frame Notation

$\bar{B}>$ body axis frame, fixed by initial conditions

$\bar{F}>$ inertially fixed frame ($\equiv \bar{f}>$)

$\bar{M}>$ sextant mirror line-of-sight frame, fixed by initial conditions

$\bar{P}>$ sextant primary line-of-sight frame, fixed by initial conditions

$\bar{R}>$ body reference frame, fixed by initial conditions

$\bar{S}$ >	true line-of-sight frame of star, fixed by initial conditions
$\bar{T}$ >	true line-of-sight frame of target, fixed by initial conditions
$\bar{b}$ >	body axis frame
$\bar{f}$ >	inertially fixed reference frame
$\bar{m}$ >	sextant mirror line-of-sight frame
$\bar{p}$ >	sextant primary line-of-sight frame
$\bar{r}$ >	body reference frame
$\bar{s}$ >	true line-of-sight frame of star
$\bar{t}$ >	true line-of-sight frame of target

Matrix Notation

I	identity matrix
k	element of matrix
M	vector rotation transformation matrix
M*	matrix with first-order terms
M**	matrix with second-order terms
M^{-1}	inverse matrix
$M_{\substack{\text{upper} \\ \text{case}}}$	fixed large angle matrix transformations (determined by intitial conditions)
x	undetermined element of matrix

Angle Notation

$\tilde{\Psi},\tilde{\Theta},\tilde{\Phi}$	total angle rotation sequence (yaw, pitch, roll)
Ψ,Θ,Φ	large angles, fixed by initial conditions
ψ,θ,φ	perturbation angles
δ	controller inputs

DESCRIPTION OF SIMULATED VEHICLE AND NAVIGATOR'S TASK

The simulated vehicle was the lunar mission vehicle illustrated in figure 1. The navigator station is located below the roll axis of the vehicle and consists, in part, of a sextant, a telescope, a sextant optics controller, and a vehicle attitude controller. The sextant primary line-of-sight axis of the sextant is fixed in the X-Z plane, 57° below the X axis. The sighting instrument has two degrees of freedom with respect to the vehicle: rotation about the primary line of sight, and pitch of the secondary with respect to the primary line of sight. These two degrees of freedom are controlled by the sextant optics controller. The direction of the primary line of sight is controlled by varying the vehicle attitude. The sextant optics controller is a proportional type which commands sextant secondary line-of-sight rate. The vehicle attitude controller is an on-off fixed-pulse type that commands vehicle attitude by discrete rate changes per pulse.

The navigator's sighting task consists of acquiring two celestial bodies, such as a star and a lunar or earth feature, in a telescope having a large field of view, and maneuvering the vehicle while actuating the optics drive so that the two bodies appear in particular areas in the telescope's field of view, where both bodies may then be seen in the limited field of view of the sextant. The navigator must then control the spacecraft so that the first celestial body is maintained near the principal reticle line (sextant measurement plane) while using the optics controller to superimpose the second body on the first; when this is accomplished he strikes the "mark" button. The mark button would presumably initiate a readout system which would record the measured angle and mission time and put this information into an on-board computer which would calculate the trajectory corrections. For this investigation, the sextant primary line of sight was chosen to be oriented on a landmark. To hold this orientation the navigator operated simulated reaction control pulse jets, mounted on the vehicle. The secondary line of sight was oriented on the desired star by the sextant optics controller. The controller rolls and pitches the secondary line of sight with respect to the primary (or shaft) axis and the trunnion axis, respectively. The sextant was assumed to have a 1.8° field of view.

Since this study was primarily concerned with system accuracy, the target was assumed to have been acquired in the sextant field of view, so the acquisition telescope was not simulated.

DESCRIPTION OF APPARATUS

The primary components of the navigation equipment proposed for the U. S. lunar mission vehicle were simulated in the fixed-cockpit simulator used in this investigation. The simulator, shown in figures 2 and 3, consisted of a seat, a vehicle attitude side-arm controller operated by the navigator's right hand, a sextant optics side-arm controller operated by his left hand, and the sighting optics and display. The simulated star-planetary target scene of

the sextant was presented on a cathode ray tube which the navigator viewed through a telescope with optical characteristics similar to those of the actual sextant telescope (×27 and 1.8° field of view). Details of the simulator system, navigator's controllers, and sextant sighting display are described below.

Simulator System Information Flow

In this simulation a hybrid analog-digital system was used consisting of an analog computer plus a "HYDAC" digital logic system shown in figure 4. Also, an analog-digital input-output system was used to command computer readout and problem recycling operations. The simulator system information flow shown in figure 5 may be described as follows. The navigator, viewing the scope display through the telescope, was provided with visual cues upon which his controller commands were based. The two-axis sextant proportional rate controller signals were fed directly into the analog computer. The three-axis vehicle pulse controller triggered the digital logic system thereby producing a fixed-amplitude, fixed-duration pulse for each axis, resulting in discrete vehicle attitude rates per pulse. The analog computer calculated the target display coordinates from the inputs from the sextant controller, vehicle rates (resulting from initial conditions and command inputs, from the vehicle attitude controller), and initial landmark line-of-sight rates. The circle generation signals (landmark display) and the coordinate information were multiplexed by the digital logic system which, in turn, fed the cathode ray tube its display information. The digital logic system also provided variable initial vehicle-rate conditions for certain portions of the study. The "mark" command put the problem in "hold" and initiated the readout and recycling operation. End-point values of angle measurement error, time to perform task, and number of control pulses used per axis were recorded.

Navigator's Controllers

The navigator's controllers can be seen in figure 3. The vehicle attitude was controlled by a two-axis pencil control for pitch and roll and a rocker plate for yaw. This type of on-off pencil controller was evaluated for space vehicle attitude control (ref. 2) and found to be quite effective. The controller was operated in a pulse command mode which resulted in a discrete angular rate being imparted to the vehicle per control pulse. A readout command (mark) switch was located just forward of the attitude controller. A finger force of 0.2 pound actuated the switch after a displacement of 0.1 inch. The vehicle attitude controller characteristics are shown in figure 6.

The sextant optics controller was a two-axis pencil controller of the proportional type. Its characteristics are shown in figure 7. Three control sensitivity levels were available, with maximum over minimum rates of 360/0.36, 3600/3.6, 36,000/36 arcsec per sec/arcsec per sec. The sensitivity selector was a three-position switch mounted just forward of the sextant controller.

The sextant controller was operated in two different modes, direct and resolved. In the direct mode, left and right stick motion commanded the roll rate of the secondary line of sight about the primary axis; forward and back motion of the stick commanded the pitch rate of the secondary line of sight about the trunnion axis. The image motion apparent to the observer in response to the stick deflection varied as a function of roll angle about the primary, or shaft, axis. In the resolved mode, the secondary line-of-sight image moves in the same direction as the controller regardless of the shaft roll angle; that is, moving the controller stick forward causes the image to move to the top of the field of view and moving it to the left causes the image to move to the left of the field, etc.

Sextant Sighting Display

For this study, the primary line of sight of the sextant was assumed to be aimed at a landmark, with the secondary line of sight being aimed at the reference star. To the observer using the sextant these two fields of view appear superposed and therefore only a single display was required for the simulation. Symbols representing the star (a dot) and the landmark (a circle) were displayed on a high quality, medium persistence cathode ray tube (fig. 8). The display was viewed through a theodolite telescope which had a magnification power of 27 and a field of view of 1.7°. A long tube was required for mounting the 5-inch oscilloscope at the proper distance in the small field of view of the telescope (fig. 2). The distance was adjusted and the oscilloscope was scaled to represent the 1.8° field of view of the actual sextant.

The minimum size dot obtainable on the cathode ray tube subtended an angle of 20 arcsec. This resulted in a 540 arcsec image at the eye, when viewed through the 27 power telescope. Data (ref. 3) indicated that images subtending less than 600 arcsec are effectively point sources of light; therefore the dot representation of a star was reasonable. Also, since the majority of the tasks required superposition of the symbols, errors in test results caused by nonlinearities in the cathode ray tube display were essentially eliminated.

The sextant reticle pattern is sketched in figure 8. Here the "R" line is the measurement reference line defining the sextant measurement plane. The "M" lines define planes perpendicular to the sextant measurement plane, with the principal "M" line passing through the center of the field of view. In an actual system, the reticle pattern rolls with respect to the navigator in response to the shaft roll-angle input from the sextant optics controller. However, for this simulation study, the reticle was rotated manually and fixed at the proper initial large angle shaft roll position. The small amount of additional reticle roll due to perturbations on the shaft roll angle was assumed to be negligible and not required for the simulation.

MATHEMATICAL MODEL DERIVATION

Symbols and Procedure

The purpose of the space sextant is to determine the angular separation between known celestial bodies to calculate spacecraft position. The mathematical model must therefore be capable of simulating the varying angular relationships due to motions of the near body, long and short period motions of the spacecraft, and sextant shaft and mirror line-of-sight angular displacement.

The mathematical model developed herein merely states in matrix form, relationships between the various frame of reference involved. The individual reference frames are expressed as orthonormal sets of basis vectors arranged in matrix form. The symbol $>$ designates a column matrix, that is,

$$\bar{b} > \equiv \begin{bmatrix} \bar{b}_1 \\ \bar{b}_2 \\ \bar{b}_3 \end{bmatrix}$$

In this way a compact expression for the transformation between frames can be made, for example,

$$\bar{b} > = M_{br} \bar{r} >$$

is short-hand notation for the expression

$$\begin{bmatrix} \bar{b}_1 \\ \bar{b}_2 \\ \bar{b}_3 \end{bmatrix} = \begin{bmatrix} k_{11} & k_{12} & k_{13} \\ k_{21} & k_{22} & k_{23} \\ k_{31} & k_{32} & k_{33} \end{bmatrix} \begin{bmatrix} \bar{r}_1 \\ \bar{r}_2 \\ \bar{r}_3 \end{bmatrix}$$

which relates the $\bar{b} >$ frame of reference to the $\bar{r} >$ frame of reference; that is, it represents a rotation of axes from the $\bar{r} >$ frame to the $\bar{b} >$ frame. Of course, the nine elements of the matrix relating the two frames are not independent; that is, only three independent variables are actually required to define all nine. The independent variables are chosen on the basis of tradition as well as of specific need. In this instance, the variables φ, θ, ψ have been chosen to represent rotations about vector axes 1, 2, and 3, respectively. Subscripts are used to define clearly each variable's place in the over-all model. Reference frame notation has been selected to be descriptive.

The matrix manipulation necessary for determining the angular relationships is illustrated by the following:

If

$$\overline{b} > = M_{br}\overline{r} >$$

$$\overline{r} > = M_{rf}\overline{f} >$$

then

$$\overline{b} > = [M_{br}M_{rf}]\overline{f} >$$

where the bracketed term is resolved by standard matrix multiplication methods. Since all the matrix transformations used in this report are between orthonormal reference frames, the inverse of each matrix is simply equal to its transpose, that is,

$$M^{-1} = M^{T}$$

Once the matrix in question is solved for, the angles relating the frames can be obtained by equating the elements of the resolved matrix to the appropriate element in the regular three angle transformation matrix. For instance, if the rotation sequence between the body and the fixed frames is defined as ψ, θ, φ (i.e., rotation order about vector axes 3, 2, and 1, respectively) then the transformation matrix would be

$$\begin{bmatrix} c\psi c\theta & s\psi c\theta & -s\theta \\ (-s\psi c\varphi + c\psi s\theta s\varphi) & (c\psi c\varphi + s\psi s\theta s\varphi) & c\theta s\varphi \\ (c\psi s\theta c\varphi + s\psi s\varphi) & (s\psi s\theta c\varphi - c\psi s\varphi) & c\theta c\varphi \end{bmatrix}$$

where s = sine, c = cosine. Then in our example

$$\theta_{bf} = -\sin^{-1}k_{13}$$

$$\psi_{bf} = \sin^{-1}\left[\frac{k_{12}}{\cos\ \theta_{bf}}\right]$$

$$\varphi_{bf} = \sin^{-1}\left[\frac{k_{23}}{\cos\ \theta_{bf}}\right]$$

Small Angle Perturbation Method Used in Rotation Matrices Multiplication

Again assume the same rotation sequence giving the rotation matrix

$$M(\psi,\theta,\varphi) = \begin{bmatrix} c\psi c\theta & s\psi c\theta & -s\theta \\ (-s\psi c\varphi + c\psi s\theta s\varphi) & (c\psi c\varphi + s\psi s\theta s\varphi) & c\theta s\varphi \\ (c\psi s\theta c\varphi + s\psi s\varphi) & (s\psi s\theta c\varphi - c\psi s\varphi) & c\theta c\varphi \end{bmatrix}$$

Now assume that the axes are rotated through small perturbation angles so that second-order series expansion for sine and cosine may be used. Then

$$\sin\theta = \theta$$

$$\cos\theta = 1 - \frac{\theta^2}{2}$$

and the rotation matrix, again to second order, becomes

$$M(\psi,\theta,\varphi) = \begin{bmatrix} \left(1 - \frac{\psi^2}{2} - \frac{\theta^2}{2}\right) & \psi & -\theta \\ (-\psi + \theta\varphi) & \left(1 - \frac{\psi^2}{2} - \frac{\varphi^2}{2}\right) & \varphi \\ \theta + \psi\varphi & (\psi\theta - \varphi) & \left(1 - \frac{\theta^2}{2} - \frac{\varphi^2}{2}\right) \end{bmatrix}$$

Breaking it into the sum of identity, first-order and second-order matrices, we get

$$M(\psi,\theta,\varphi) = \begin{bmatrix} 1 & 0 & 0 \\ 0 & 1 & 0 \\ 0 & 0 & 1 \end{bmatrix} + \begin{bmatrix} 0 & \psi & -\theta \\ -\psi & 0 & \varphi \\ \theta & -\varphi & 0 \end{bmatrix} + \begin{bmatrix} \left(-\frac{\psi^2}{2} - \frac{\theta^2}{2}\right) & 0 & 0 \\ \theta\varphi & \left(-\frac{\psi^2}{2} - \frac{\varphi^2}{2}\right) & 0 \\ \psi\varphi & \psi\theta & \left(-\frac{\theta^2}{2} - \frac{\varphi^2}{2}\right) \end{bmatrix}$$

$$= I + M^* + M^{**} \qquad (1)$$

Further expanded, the above matrix becomes

$$M^* = \begin{bmatrix} 0 & \psi & -\theta \\ -\psi & 0 & \varphi \\ \theta & -\varphi & 0 \end{bmatrix} = \psi \begin{bmatrix} 0 & 1 & 0 \\ -1 & 0 & 0 \\ 0 & 0 & 0 \end{bmatrix} + \theta \begin{bmatrix} 0 & 0 & -1 \\ 0 & 0 & 0 \\ 1 & 0 & 0 \end{bmatrix} + \varphi \begin{bmatrix} 0 & 0 & 0 \\ 0 & 0 & 1 \\ 0 & -1 & 0 \end{bmatrix}$$

$$M^{**} = \begin{bmatrix} \left(-\frac{\psi^2}{2} - \frac{\theta^2}{2}\right) & 0 & 0 \\ \theta\varphi & \left(-\frac{\psi^2}{2} - \frac{\varphi^2}{2}\right) & 0 \\ \psi\varphi & \psi\theta & \left(-\frac{\theta^2}{2} - \frac{\varphi^2}{2}\right) \end{bmatrix}$$

$$= \frac{\psi^2}{2} \begin{bmatrix} -1 & 0 & 0 \\ 0 & -1 & 0 \\ 0 & 0 & 0 \end{bmatrix} + \frac{\theta^2}{2} \begin{bmatrix} -1 & 0 & 0 \\ 0 & 0 & 0 \\ 0 & 0 & -1 \end{bmatrix} + \frac{\varphi^2}{2} \begin{bmatrix} 0 & 0 & 0 \\ 0 & -1 & 0 \\ 0 & 0 & -1 \end{bmatrix}$$

$$+ \varphi\theta \begin{bmatrix} 0 & 0 & 0 \\ 1 & 0 & 0 \\ 0 & 0 & 0 \end{bmatrix} + \varphi\psi \begin{bmatrix} 0 & 0 & 0 \\ 0 & 0 & 0 \\ 1 & 0 & 0 \end{bmatrix} + \theta\psi \begin{bmatrix} 0 & 0 & 0 \\ 0 & 0 & 0 \\ 0 & 1 & 0 \end{bmatrix}$$

Introduction to Reference Frames

All reference frames are defined directly or indirectly with respect to one reference frame fixed in inertial space. This reference frame is denoted

$$\overline{f} > = \begin{bmatrix} \overline{f}_1 \\ \overline{f}_2 \\ \overline{f}_3 \end{bmatrix}$$

where (see fig. 9)

$\bar{f}_1$ unit vector directed along the vernal equinox line

$\bar{f}_3$ unit vector directed toward the north celestial pole

$\bar{f}_2$ unit vector orthogonal to both $\bar{f}_1$ and $\bar{f}_3$ in the usual right-hand sense

All reference frames are orthonormal sets of basis vectors spanning 3 space. The total angle rotation sequence chosen is $\tilde{\Psi}$, $\tilde{\Theta}$, $\tilde{\Phi}$. Subscripts refer to the frames involved, that is, M_{sm} implies $\bar{s}>$ with respect to $\bar{m}>$.

A tabulation of the transformations which are used is as follows:

$\bar{r}> = M_{rf}\bar{f}>$; $M_{rf}(\tilde{\Psi}_{rf}, \tilde{\Theta}_{rf}, \tilde{\Phi}_{rf})$ (fig. 9)

$\bar{b}> = M_{br}\bar{r}>$; $M_{br}(\tilde{\Psi}_{br}, \tilde{\Theta}_{br}, \tilde{\Phi}_{br})$ (fig. 10)

$\bar{p}> = M_{pb}\bar{b}>$; $M_{pb}(\tilde{\Theta}_{pb}, \tilde{\Phi}_{pb})$ (fig. 11)

$\bar{m}> = M_{mp}\bar{p}>$; $M_{mp}(\tilde{\Theta}_{mp})$ (fig. 12)

$\bar{s}> = M_{sr}\bar{r}>$; $M_{sr}(\tilde{\Psi}_{sr}, \tilde{\Theta}_{sr}, \tilde{\Phi}_{sr})$ (figs. 10, 11, 12)

$\bar{t}> = M_{tr}\bar{r}>$; $M_{tr}(\tilde{\Psi}_{tr}, \tilde{\Theta}_{tr}, \tilde{\Phi}_{tr})$ (figs. 10, 11, 12)

The relationships between the matrix transformations, the rotation angle inputs to the matrix transformations, and the reference frames are shown in figure 13. The rotation angle outputs which are found by solving for the unknown matrix transformations are also shown.

Solution for Star Display Angles

The star display perturbation angles θ_{sm} and ψ_{sm} in figure 13 are obtained in the following manner:

$$\left.\begin{aligned} M_{sr} &= M_{sm}M_{mp}M_{pb}M_{br} \\ M_{sm} &= M_{sr}[M_{mp}M_{pb}M_{br}]^{-1} \end{aligned}\right\} \qquad (2)$$

When the mirror line of sight ($\bar{m}>$) coincides with the true star line of sight ($\bar{s}>$),

$$M_{sm} = I \quad \text{(the identity matrix)}$$

and M_{sr} can be determined. Assume that above is true for initial large angle conditions. Then

$$M_{sr} = M_{MP}M_{PB}M_{BR}$$

where these matrices are functions of the initial large angles

$$M_{MP}(\Theta_{mp})$$

$$M_{PB}(\Theta_{pb},\Phi_{pb})$$

Also assume that $\overline{r} > = \overline{b} >$ initially, so

$$M_{BR} = I$$

then

$$M_{sr} = M_{MP}M_{PB}$$

which is assumed to be constant for a given initial star-landmark acquisition case, and does not affect the problem within a certain degree of accuracy, when the input angles are perturbed through small additional angles. Therefore

$$M_{sm} = M_{MP}M_{PB}[M_{mp}M_{pb}M_{br}]^{-1}$$

or in the form actually used in the development

$$M_{sm}^{-1} = M_{mp}M_{pb}M_{br}[M_{MP}M_{PB}]^{-1} \qquad (3)$$

Let

Ψ, Θ, Φ = initial large angles

ψ, θ, φ = perturbation angles

and assume that a total angle transformation can be broken up as

$$M(\text{total angles}) = M(\psi,\theta,\varphi)M(\Psi,\Theta,\Phi)$$

that is, a rotation through the large angles followed by perturbation angle rotations.

So

$$M_{sm}^{-1} = M_{mp}(\theta_{mp})M_{MP}(\Theta_{mp})M_{pb}(\varphi_{pb})M_{PB}(\Phi_{pb})M_{PB}(\Theta_{pb})$$

$$M_{br}(\varphi_{br})M_{br}(\theta_{br})M_{br}(\psi_{br})[M_{PB}^{-1}(\Theta_{pb})M_{PB}^{-1}(\Phi_{pb})M_{MP}^{-1}(\Theta_{mp})] \qquad (4)$$

Now using the second-order perturbation angle matrices as outlined in the section Symbols and Procedure (eq. (1)), expand the equation to

$$M_{sm}^{-1} = \left\{ I + \theta_{mp}\begin{bmatrix} 0 & 0 & -1 \\ 0 & 0 & 0 \\ 1 & 0 & 0 \end{bmatrix} + \frac{1}{2}\theta_{mp}^2 \begin{bmatrix} -1 & 0 & 0 \\ 0 & 0 & 0 \\ 0 & 0 & -1 \end{bmatrix} \right\} M_{MP}(\Theta_{mp})$$

$$\left\{ I + \varphi_{pb}\begin{bmatrix} 0 & 0 & 0 \\ 0 & 0 & 1 \\ 0 & -1 & 0 \end{bmatrix} + \frac{1}{2}\varphi_{pb}^2 \begin{bmatrix} 0 & 0 & 0 \\ 0 & -1 & 0 \\ 0 & 0 & -1 \end{bmatrix} \right\} \left\{ M_{PB}(\Phi_{pb})M_{PB}(\Theta_{pb}) \right\}$$

$$\left\{ I + \varphi_{br}\begin{bmatrix} 0 & 0 & 0 \\ 0 & 0 & 1 \\ 0 & -1 & 0 \end{bmatrix} + \theta_{br}\begin{bmatrix} 0 & 0 & -1 \\ 0 & 0 & 0 \\ 1 & 0 & 0 \end{bmatrix} + \psi_{br}\begin{bmatrix} 0 & 1 & 0 \\ -1 & 0 & 0 \\ 0 & 0 & 0 \end{bmatrix} \right.$$

$$+ \frac{1}{2}\theta_{br}^2 \begin{bmatrix} -1 & 0 & 0 \\ 0 & 0 & 0 \\ 0 & 0 & -1 \end{bmatrix} + \frac{1}{2}\psi_{br}^2 \begin{bmatrix} -1 & 0 & 0 \\ 0 & -1 & 0 \\ 0 & 0 & 0 \end{bmatrix} + \frac{1}{2}\varphi_{br}^2 \begin{bmatrix} 0 & 0 & 0 \\ 0 & -1 & 0 \\ 0 & 0 & -1 \end{bmatrix}$$

$$\left. + \varphi_{br}\theta_{br}\begin{bmatrix} 0 & 0 & 0 \\ 1 & 0 & 0 \\ 0 & 0 & 0 \end{bmatrix} + \varphi_{br}\psi_{br}\begin{bmatrix} 0 & 0 & 0 \\ 0 & 0 & 0 \\ 1 & 0 & 0 \end{bmatrix} + \theta_{br}\psi_{br}\begin{bmatrix} 0 & 0 & 0 \\ 0 & 0 & 0 \\ 0 & 1 & 0 \end{bmatrix} \right\}$$

$$\left\{ M_{PB}^{-1}(\Theta_{pb})M_{pb}^{-1}(\Phi_{pb})M_{MP}^{-1}(\Theta_{mp}) \right\} \qquad (5)$$

Also from equation (1)

$$M_{sm}^{-1} = I + M_{sm}^{*-1} + M_{sm}^{**-1} \tag{6}$$

$$M_{sm}^{*-1} = \begin{bmatrix} 0 & -\psi & \theta \\ \psi & 0 & -\varphi \\ -\theta & \varphi & 0 \end{bmatrix}_{sm}$$

$$M_{sm}^{**-1} = \begin{bmatrix} -\left(\frac{\psi^2}{2} + \frac{\theta^2}{2}\right) & \theta\varphi & \psi\varphi \\ 0 & -\left(\frac{\psi^2}{2} + \frac{\varphi^2}{2}\right) & \psi\theta \\ 0 & 0 & -\left(\frac{\theta^2}{2} + \frac{\varphi^2}{2}\right) \end{bmatrix}_{sm}$$

Now solve for θ_{sm}, ψ_{sm}, φ_{sm} the star display angles, by equating (5) and (6) and noting that

$$-\theta_{sm} = \sum k_{31}$$

$$\psi_{sm} = \sum k_{21}$$

$$\varphi_{sm} = \sum k_{32}$$

where the subscripts refer to the row and column (e.g., 31 means row 3 column 1). Let

$$A = M_{MP}(\Theta_{mp})$$

$$C = M_{PB}(\Theta_{pb}, \Phi_{pb})$$

and letting the appropriate matrices multiplying the variables be understood, write equation (5) in short-hand form

$$M_{sm}^{-1} = \left\{I + \theta_{mp} + \frac{1}{2}\theta_{mp}^2\right\} A \left\{I + \varphi_{pb} + \frac{1}{2}\varphi_{pb}^2\right\}$$

$$B \left\{I + \varphi_{br} + \theta_{br} + \psi_{br} + \frac{1}{2}\theta_{br}^2 + \frac{1}{2}\psi_{br}^2\right.$$

$$\left. + \frac{1}{2}\varphi_{br}^2 + \varphi_{br}\theta_{br} + \varphi_{br}\psi_{br} + \theta_{br}\psi_{br}\right\} C^{-1}A^{-1}$$

Then to second order

$$M_{sm}^{-1} = \left\{A + A\varphi_{pb} + A\frac{1}{2}\varphi_{pb}^2 + \theta_{mp}A + \theta_{mp}A\varphi_{pb}\right.$$

$$\left. + \frac{1}{2}\theta_{mp}^2 A\right\} \left\{A^{-1} + C\varphi_{br}C^{-1}A^{-1} + B\theta_{br}C^{-1}A^{-1} + B\psi_{br}C^{-1}A^{-1}\right.$$

$$+ C\frac{1}{2}\theta_{br}^2 C^{-1}A^{-1} + C\frac{1}{2}\psi_{br}^2 C^{-1}A^{-1} + C\frac{1}{2}\varphi_{br}^2 C^{-1}A^{-1}$$

$$\left. + C\varphi_{br}\theta_{br}C^{-1}A^{-1} + C\varphi_{br}\psi_{br}C^{-1}A^{-1} + C\theta_{br}\psi_{br}C^{-1}A^{-1}\right\}$$

Again to second order and noting that

$$MM^{-1} = I$$

we have

$$M_{sm}^{-1} = I + AC\varphi_{br}C^{-1}A^{-1} + AC\theta_{br}C^{-1}A^{-1} + AC\psi_{br}C^{-1}A^{-1} + AC\frac{1}{2}\theta_{br}^2 C^{-1}A^{-1}$$

$$+ AC\frac{1}{2}\psi_{br}C^{-1}A^{-1} + AC\frac{1}{2}\varphi_{br}^2 C^{-1}A^{-1} + AC\varphi_{br}\theta_{br}C^{-1}A^{-1} + AC\varphi_{br}\psi_{br}C^{-1}A^{-1}$$

$$+ AC\theta_{br}\psi_{br}C^{-1}A^{-1} + A\varphi_{pb}A^{-1} + A\varphi_{pb}A^{-1}AC\varphi_{br}C^{-1}A^{-1} + A\varphi_{pb}A^{-1}AC\theta_{br}C^{-1}A^{-1}$$

$$+ A\varphi_{pb}A^{-1}AC\psi_{br}C^{-1}A^{-1} + A\frac{1}{2}\varphi_{pb}^2 A^{-1} + \theta_{mp} + \theta_{mp}AC\varphi_{br}C^{-1}A^{-1}$$

$$+ \theta_{mp}AC\theta_{br}C^{-1}A^{-1} + \theta_{mp}AC\psi_{br}C^{-1}A^{-1} + \theta_{mp}A\varphi_{pb}A^{-1} + \frac{1}{2}\theta_{mp}^2 \qquad (5a)$$

Term by term, equation (5a) becomes as shown in appendix A.

Solution for Landmark Display Angles

As indicated in figure 13, the landmark display angles θ_{tp} and ψ_{tp} are obtained in a manner similar to that for the star display angles.

$$M_{tr} = M_{tp}M_{pb}M_{br}$$

Then

$$M_{tp} = M_{tr}[M_{pb}M_{br}]^{-1}$$

or

$$M_{tp}^{-1} = M_{pb}M_{br}M_{tr}^{-1}$$

When the shaft line of sight ($\overline{p}_1 >$) coincides with the true landmark target line of sight ($\overline{t}_1 >$),

$$M_{tp} = I$$

and M_{tr} can be determined. Assume that this is true for initial large angle conditions. Then initially

$$M_{tr} = M_{PB}M_{BR}$$

where, again, these matrices are functions of the initial large angles, and as before

$$M_{BR} = I$$

so

$$M_{tr} = M_{PB}$$

initially. Now let the landmark line-of-sight frame be perturbed through small angles with respect to the initial shaft axis system, representing near body motion (see fig. 13)

$$M_{tr} = M_{tP}M_{PB}$$

so

$$M_{tp}^{-1} = M_{pb}M_{br}[M_{tP}M_{PB}]^{-1} = M_{pb}M_{br}M_{PB}^{-1}M_{tP}^{-1} \qquad (7)$$

where M_{tP} is the perturbation matrix.

Again using perturbation angles and equation (1), in equation (7), we have

$$M_{tp}^{-1} = M_{pb}(\varphi_{pb})M_{PB}(\Phi_{pb})M_{PB}(\Theta_{pb})M(\varphi_{br})M(\theta_{br})M(\psi_{br})$$

$$M_{pB}^{-1}(\Theta_{pb})M_{PB}^{-1}(\Phi_{pb})M_{tr}^{-1}(\psi_{tr})M_{tP}^{-1}(\theta_{tP})M_{tP}^{-1}(\varphi_{tP})$$

$$= \left\{ I + \varphi_{pb} \begin{bmatrix} 0 & 0 & 0 \\ 0 & 0 & 1 \\ 0 & -1 & 0 \end{bmatrix} + \frac{1}{2}\varphi_{pb}^2 \begin{bmatrix} 0 & 0 & 0 \\ 0 & -1 & 0 \\ 0 & 0 & -1 \end{bmatrix} \right\} M_{PB}(\Phi_{pb})M_{PB}(\Theta_{pb})$$

$$\left\{ I + \varphi_{br} \begin{bmatrix} 0 & 0 & 0 \\ 0 & 0 & 1 \\ 0 & -1 & 0 \end{bmatrix} + \theta_{br} \begin{bmatrix} 0 & 0 & -1 \\ 0 & 0 & 0 \\ 1 & 0 & 0 \end{bmatrix} + \psi_{br} \begin{bmatrix} 0 & 1 & 0 \\ -1 & 0 & 0 \\ 0 & 0 & 0 \end{bmatrix} + \frac{1}{2}\varphi_{br}^2 \begin{bmatrix} 0 & 0 & 0 \\ 0 & -1 & 0 \\ 0 & 0 & -1 \end{bmatrix} \right.$$

$$+ \frac{1}{2}\theta_{br}^2 \begin{bmatrix} -1 & 0 & 0 \\ 0 & 0 & 0 \\ 0 & 0 & -1 \end{bmatrix} + \frac{1}{2}\psi_{br}^2 \begin{bmatrix} -1 & 0 & 0 \\ 0 & -1 & 0 \\ 0 & 0 & 0 \end{bmatrix} + \varphi_{br}\theta_{br} \begin{bmatrix} 0 & 0 & 0 \\ 1 & 0 & 0 \\ 0 & 0 & 0 \end{bmatrix}$$

$$\left. + \varphi_{br}\psi_{br} \begin{bmatrix} 0 & 0 & 0 \\ 0 & 0 & 0 \\ 1 & 0 & 0 \end{bmatrix} + \theta_{br}\psi_{br} \begin{bmatrix} 0 & 0 & 0 \\ 0 & 0 & 0 \\ 0 & 1 & 0 \end{bmatrix} \right\} M_{PB}^{-1}(\Theta_{pb})M_{PB}^{-i}(\Phi_{pb})$$

$$\left\{ I + \psi_{tP} \begin{bmatrix} 0 & -1 & 0 \\ 1 & 0 & 0 \\ 0 & 0 & 0 \end{bmatrix} + \theta_{tP} \begin{bmatrix} 0 & 0 & 1 \\ 0 & 0 & 0 \\ -1 & 0 & 0 \end{bmatrix} + \varphi_{tP} \begin{bmatrix} 0 & 0 & 0 \\ 0 & 0 & -1 \\ 0 & 1 & 0 \end{bmatrix} \right.$$

$$+ \frac{1}{2}\psi_{tP}^2 \begin{bmatrix} -1 & 0 & 0 \\ 0 & -1 & 0 \\ 0 & 0 & 0 \end{bmatrix} + \frac{1}{2}\theta_{tP}^2 \begin{bmatrix} -1 & 0 & 0 \\ 0 & 0 & 0 \\ 0 & 0 & -1 \end{bmatrix} + \frac{1}{2}\varphi_{tP}^2 \begin{bmatrix} 0 & 0 & 0 \\ 0 & -1 & 0 \\ 0 & 0 & -1 \end{bmatrix}$$

$$\left. + \varphi_{tP}\theta_{tP} \begin{bmatrix} 0 & 1 & 0 \\ 0 & 0 & 0 \\ 0 & 0 & 0 \end{bmatrix} + \varphi_{tP}\psi_{tP} \begin{bmatrix} 0 & 0 & 1 \\ 0 & 0 & 0 \\ 0 & 0 & 0 \end{bmatrix} + \theta_{tP}\psi_{tP} \begin{bmatrix} 0 & 0 & 0 \\ 0 & 0 & 1 \\ 0 & 0 & 0 \end{bmatrix} \right\} \qquad (8)$$

Again by equation (1)

$$M_{tp}^{-1} = I + M_{tp}^{*-1} + M_{tp}^{**-1} \tag{9}$$

$$M_{tp}^{*-1} = \begin{bmatrix} 0 & -\psi & \theta \\ \psi & 0 & -\varphi \\ -\theta & \varphi & 0 \end{bmatrix}_{tp}$$

$$M_{tp}^{**-1} = \begin{bmatrix} -\left(\frac{\psi^2}{2} + \frac{\theta^2}{2}\right) & \theta\varphi & \psi\varphi \\ 0 & -\left(\frac{\psi^2}{2} + \frac{\varphi^2}{2}\right) & \psi\theta \\ 0 & 0 & -\left(\frac{\theta^2}{2} + \frac{\varphi^2}{2}\right) \end{bmatrix}_{tp}$$

Now the landmark display angles can be found by equating (8) and (9) and noting that

$$-\theta_{tp} = \sum k_{31}$$

$$\psi_{tp} = \sum k_{21}$$

$$\varphi_{tp} = \sum k_{32}$$

Forming the products called for in (8), cancelling third-order and higher terms, and using the fact that

$$MM^{-1} = I$$

changes equation (8), term by term, as shown in appendix A.

Solution for True Angle and Error

The sighting error is defined as the difference between the sighting angle read by the navigator using the sextant and the true angle.

$$\text{error} = \tilde{\Theta}_{mp} - \tilde{\Theta}_{st} \tag{10}$$

Because of near body and spacecraft trajectory motion, the true angle between a star and a landmark is continually varying. Therefore the perturbations of the true angle must be expressed as a function of the time varying target positions. The true angle is defined here as the angle between $\bar{t}_1$ and $\bar{s}_1$. The transformation matrix between the $\bar{t}>$ frame and the $\bar{s}>$ frame for a rotation angle sequence, roll, pitch, roll, is

$$M_{st} = M(\tilde{\Phi}_1, \tilde{\Theta}, \tilde{\Phi}_2)$$

where ~ indicates total angles. Thus,

$$M_{st} = \begin{bmatrix} c\tilde{\Theta} & s\tilde{\Phi}_1 s\tilde{\Theta} & c\tilde{\Phi}_1 s\tilde{\Theta} \\ s\tilde{\Theta}s\tilde{\Phi}_2 & c\tilde{\Phi}_1 c\tilde{\Phi}_2 - s\tilde{\Phi}_1 c\tilde{\Theta}s\tilde{\Phi}_2 & s\tilde{\Phi}_1 c\tilde{\Phi}_2 + c\tilde{\Phi}_1 c\tilde{\Theta}s\tilde{\Phi}_2 \\ s\tilde{\Theta}c\tilde{\Phi}_2 & -c\tilde{\Phi}_1 s\tilde{\Phi}_2 - s\tilde{\Phi}_1 c\tilde{\Theta}c\tilde{\Phi}_2 & -s\tilde{\Phi}_1 s\tilde{\Phi}_2 + c\tilde{\Phi}_1 c\tilde{\Theta}c\tilde{\Phi}_2 \end{bmatrix} \tag{11}$$

From figure 13, we can also write the transformation using the matrix loop

$$M_{sr} = M_{st}M_{tr}$$

or

$$M_{st} = M_{sr}M_{tr}^{-1}$$

From the solution for star display angles

$$M_{sr} = M_{MP}M_{PB}$$

and from the solution for landmark display angles

$$M_{tr} = M_{tP}M_{PB}$$

Then

$$M_{st} = M_{MP} M_{PB} M_{PB}^{-1} M_{tP}^{-1}$$

$$M_{st} = M_{MP} M_{tP}^{-1} \tag{12}$$

Equation (1) is used to write equation (12) as

$$M_{st} = M_{MP} \left\{ I + \varphi_{tP} \begin{bmatrix} 0 & 0 & 0 \\ 0 & 0 & -1 \\ 0 & 1 & 0 \end{bmatrix} + \theta_{tP} \begin{bmatrix} 0 & 0 & 1 \\ 0 & 0 & 0 \\ -1 & 0 & 0 \end{bmatrix} + \psi_{tP} \begin{bmatrix} 0 & -1 & 0 \\ 1 & 0 & 0 \\ 0 & 0 & 0 \end{bmatrix} \right.$$

$$+ \frac{1}{2} \theta_{tP}^2 \begin{bmatrix} -1 & 0 & 0 \\ 0 & 0 & 0 \\ 0 & 0 & -1 \end{bmatrix} + \frac{1}{2} \psi_{tP}^2 \begin{bmatrix} -1 & 0 & 0 \\ 0 & -1 & 0 \\ 0 & 0 & 0 \end{bmatrix} + \frac{1}{2} \varphi_{tP}^2 \begin{bmatrix} 0 & 0 & 0 \\ 0 & -1 & 0 \\ 0 & 0 & -1 \end{bmatrix}$$

$$\left. + \varphi_{tP}\theta_{tP} \begin{bmatrix} 0 & 1 & 0 \\ 0 & 0 & 0 \\ 0 & 0 & 0 \end{bmatrix} + \varphi_{tP}\psi_{tP} \begin{bmatrix} 0 & 0 & 1 \\ 0 & 0 & 0 \\ 0 & 0 & 0 \end{bmatrix} \theta_{tP}\psi_{tP} \begin{bmatrix} 0 & 0 & 0 \\ 0 & 0 & 1 \\ 0 & 0 & 0 \end{bmatrix} \right\} \tag{13}$$

Equating elements k_{11} of equations (11) and (13) results in a solution for the star-landmark separation angle

$$c\tilde{\Theta}_{st} = c\Theta_{mp} + \theta_{tP} s\Theta_{mp} - \frac{1}{2} \theta_{tP}^2 c\Theta_{mp} - \frac{1}{2} \psi_{tP}^2 c\Theta_{mp} \tag{14}$$

Now break up $\tilde{\Theta}_{st}$ into large angles plus a perturbation angle

$$\tilde{\Theta}_{st} = \Theta_{st} + \theta_{st}$$

$$= \Theta_{mp} + \theta_{st}$$

Then

$$\cos \tilde{\Theta}_{st} = \cos[\Theta_{mp} + \theta_{st}]$$

$$= c\Theta_{mp}c\theta_{st} - s\Theta_{mp}s\theta_{st}$$

which to second order is

$$c\tilde{\Theta}_{st} = c\Theta_{mp}\left(1 - \frac{1}{2}\theta_{st}^2\right) - s\Theta_{mp}\theta_{st}$$

$$= c\Theta_{mp} - \frac{1}{2}\theta_{st}^2 c\Theta_{mp} - \theta_{st}s\Theta_{mp} \qquad (15)$$

Equating equations (14) and (15) gives

$$c\Theta_{mp} + \theta_{tP}s\Theta_{mp} - \frac{1}{2}\theta_{tP}^2 c\Theta_{mp} - \frac{1}{2}\psi_{tP}^2 c\Theta_{mp} = c\Theta_{mp} - \frac{1}{2}\theta^2{}_{st}c\Theta_{mp} - \theta_{st}s\Theta_{mp} \qquad (16)$$

which is a quadratic equation in θ_{st}. To facilitate the solution of equation (16) on the analog computer, we assumed the perturbation terms, θ_{tP}^2 and θ_{st}^2 to cancel each other. Calculations showed no degradation in simulation accuracy to result from this approximation. Equation (16) then becomes

$$\theta_{st} = -\theta_{tP} + \psi_{tP}^2\left(\frac{1}{2}\tan \Theta_{mp}\right) \qquad (17)$$

which is the desired true angle perturbation.

TYPICAL RESULTS

The simulation setup just described was used for collecting a considerable amount of data illustrating the performance of the navigator-sextant combination. The bulk of these data was presented in reference 1. However, some typical data are repeated herein to help illustrate the usefulness and versatility of the sextant simulator. The performance criteria for this simulation program were: (a) accuracy of the sighting angle measurement as indicated by the standard deviation of the error for a series of sightings, (b) amount of fuel used during the sighting as indicated by the average number of vehicle controller pulses per axis, and (c) the average time to complete a sighting. The results shown here are: basic sighting accuracy, effects of target motion, and effects of vehicle attitude and target motion.

The initial large values of shaft roll angle, mirror pitch angle, and initial vehicle attitude angles were preselected and the effects of perturbations about these initial angles were studied. Initial sextant angle conditions could be varied, but for the bulk of the program it was assumed that a shaft roll angle of 45° and a mirror or trunnion pitch angle of 45° represented a typical situation. For all runs, the sextant secondary line-of-sight shaft and trunnion perturbation angles were offset $1/4^{\circ}$ each, that is, the star image was offset from the principal M line and the R line by $1/4^{\circ}$. For a given set of conditions, the subject repeated the sighting problem from 16 to 20 times, to provide a statistical basis for the study of the effects on performance of a particular parameter variation.

Base-line sighting accuracy.- To determine the best sighting accuracy that could be expected, some basic accuracy sightings were made and repeated with all effects of vehicle or target motion eliminated. The data for this idealized condition are presented in figure 14. The test conditions were: fixed vehicle attitude, no landmark motion, 20 arcsec dot with a 50 arcsec circle, and a low speed on the optics controller. Sextant roll angle was fixed at 0°, and the operator controlled only the sextant pitch or trunnion angle. This was done to eliminate off-plane sighting errors (described below). The basic accuracy or repeatability of the system when the dot is being superimposed in the center of the circle had a 1σ value of 2 arcsec or less. Learning time was negligible and navigator performance did not seem to deteriorate appreciably even when many days lapsed between sightings.

Sextant off-plane sighting errors.- In general, a sextant will measure the true angle formed by two targets and the observer only when the two images are superimposed and positioned on the R line, that is, in the sextant measurement plane. The superposition does not have to occur at any specific position along the R line. Because of the image motion caused by a moving landmark line of sight or vehicle motion, a perfect measurement reading may become too time consuming or, at very high rates, impossible. Therefore a certain amount of error will always be present in the sextant measurement as a result of the images being off-plane, that is, away from the R line. A theoretical study of these out-of-plane measurement errors has been developed and is presented in appendix B. The theoretical results show that sighting at small off-plane angles can be tolerated. For instance, with the landmark and star superposed off-plane by a lateral angle equal to 10 percent of the 1.8° field of view, the error in sighting measurement for a measured angle of 45° is less than 1 arcsec.

Effect of landmark line-of-sight motion.- Effects of landmark motion with vehicle control active are shown in figure 15. In this and subsequent figures, in-plane motion refers to landmark line-of-sight motion in the mirror pitch plane, that is, parallel to the sextant measurement plane. Ortho-plane motion refers to landmark line-of-sight motion perpendicular to the sextant measurement plane. Vehicle attitude controller sensitivities in this portion of the study correspond to the minimum rate per pulse values expected for a typical vehicle in the transearth portion of a lunar mission, that is, yaw and pitch rates of 80 arcsec/sec per pulse, and roll rates of 320 arcsec/sec per pulse.

Midcourse sightings: For the major portion of the midcourse phase of a lunar mission, the earth or moon landmark line-of-sight rates will be less than 20 arcsec/sec of time. This low rate has negligible effect upon sighting performance for the system studied, as illustrated in figure 15. Accuracy levels remained close to those for a fixed landmark and vehicle, the base-line standard deviation of 2 arcsec or less. Therefore, if a normal distribution is assumed and the vehicle rates are near zero, the system accuracy for the midcourse phase can be expected to be ±6 arcsec (3σ) for 99.7 percent of the sightings. Sighting times after acquisition averaged 10 to 15 seconds.

Close-in sightings: For "close-in" sightings, outside the midcourse range (approximately 25,000 to 380,000 km from earth), the increased landmark line-of-sight rate causes considerable error. If a 3σ (99.7-percent level) value of 10 arcsec is assumed as a minimum required accuracy level, landmark line-of-sight rates must be less than 280 arcsec/sec for in-plane or ortho-plane motion, and must result in a rate of less than 280 arcsec/sec for combined in-plane and ortho-plane motion.

A summary of the data, including conditions with the controller inactive (i.e., fixed vehicle), at selected combined landmark rates of 20, 200, and 400 arcsec/sec, is shown in table I.

Effect of combined landmark and vehicle motions.- During an actual space flight both the landmark and the vehicle attitude will move during the sighting task. Performance of the navigator sextant with both landmark line-of-sight motion and a particular set of vehicle attitude rates is shown in figures 16 to 18 for this simulation study. The control sensitivities which were used were 320, 80, and 80 arcsec/sec per pulse for roll, pitch, and yaw, respectively. These control sensitivities were chosen because they are the expected values for the lunar vehicle on its return or transearth phase. The initial vehicle rates chosen were half of these control sensitivity rates, and therefore at least these minimum rates were always present. Combining these initial attitude rates gives a resultant rate of 170 arcsec/sec.

As mentioned, lunar mission midcourse landmark line-of-sight rates will be less than 17 arcsec/sec. Using the expected flight values with the data of figure 16 shows that system accuracy with both landmark and vehicle motion (170 arcsec/sec minimum) can be expected to be ±8 arcsec (3σ) for the midcourse phase. This can be compared with ±6 arcsec for the zero vehicle rate condition (fig. 15). Outside the midcourse phase, except for subject 4, the maximum allowable landmark line-of-sight rate, based on the 10 arcsec (3σ) criteria, was again 280 arcsec/sec, the same as for the zero initial vehicle rate of figure 15. To determine whether performance was affected by the navigator's adaptation to repeated initial conditions, the study was repeated for two subjects with random sign combinations of the initial vehicle rates. As shown in figure 16, the performance accuracy was about the same. Sighting times (fig. 17) were similar for both the repeated conditions and the random sign conditions. The pulse data (fig. 18) also showed no significant difference for the two subjects.

Performance values for landmark rates of 20, 200, and 400 arcsec/sec both with and without initial vehicle attitude rates are presented in table I.

The data are similar except that, with initial vehicle rate, more pulses are required because of the noncancellable vehicle attitude rates.

CONCLUSIONS

A detailed description has been given of the mathematical model and simulator implementation for a fixed-base vehicle-mounted, navigator-controlled space sextant simulator. It was found that a computation accuracy of 1 arcsec could be obtained on a conventional analog computer, by approximating the system rotational kinematics with second-order perturbation angle techniques. The navigator station simulator incorporated a simple telescope, a cathode ray tube display, and two side-arm controllers. With this relatively inexpensive hardware and an analog computer with a digital logic system, an over-all "man-in-the-loop" basic simulator accuracy of 2 arcsec was obtained. Some typical data of the navigator-space sextant combination performance study were presented.

Ames Research Center
National Aeronautics and Space Administration
Moffett Field, Calif., Mar. 8, 1965

REFERENCES

1. Kurkowski, Richard L.; and Grover, Kenneth C.: A Study of the Navigator's Sighting Accuracy Using a Simulated Vehicle-Mounted Space Sextant and a Description of the Sextant Simulator. Paper for AIAA/ION, Astrodynamics, Guidance and Control Conference, UCLA, Los Angeles, Calif., Aug. 24-26, 1964.

2. Lopez, Armando E.; and Smith, Donald W.: Simulator Studies of the Manual Control of Vehicle Attitude Using an On-Off Reaction Control System. NASA TN D-2068, 1963.

3. Blackwell, H. R.: Contrast Thresholds of the Human Eye. Opt. Soc. of Am. J., vol. 36, 1946, pp. 624-643.

APPENDIX A

SUMMARY OF EQUATIONS

Scope Display Angles

		Associated parameter coefficient series
$-\theta_{sm} = \sum k_{31}$	of M_{sm}^{-1}	100
$\psi_{sm} = \sum k_{21}$	of M_{sm}^{-1}	200
$\varphi_{sm} = \sum k_{32}$	of M_{sm}^{-1}	300
$-\theta_{tp} = \sum k_{31}$	of M_{tp}^{-1}	400
$\psi_{tp} = \sum k_{21}$	of M_{tp}^{-1}	500
$\varphi_{tp} = \sum k_{32}$	of M_{tp}^{-1}	600

where the subscripts refer to the row and column (e.g., 31 means row 3 column 1). Now we define the parameter coefficients as

$$a_{101}, a_{102}, a_{103}, \ldots$$

$$a_{201}, a_{202}, a_{203}, \ldots$$

etc.

where the 100 series refers to elements k_{31} associated with Θ_{sm}, the 200 series to the element k_{21} associated with ψ_{sm}, etc. The tens and unit digit refer to the independent parameter number, that is,

$$01 \text{ -- } _{br}, \; 02 \text{ -- } _{br}, \ldots$$

The equations can then be summarized as:

$$-\theta_{sm} = a_{101}\varphi_{br} + a_{102}\theta_{br} + a_{103}\psi_{br} + a_{104}\varphi_{pb} + a_{105}\theta_{mp} + a_{106}\frac{1}{2}\varphi_{br}^2$$
$$+ a_{107}\frac{1}{2}\theta_{br}^2 + a_{108}\frac{1}{2}\psi_{br}^2 + a_{109}\frac{1}{2}\varphi_{pb}^2 + a_{110}\frac{1}{2}\theta_{mp}^2$$
$$+ a_{111}\varphi_{br}\theta_{br} + a_{112}\varphi_{br}\psi_{br} + a_{113}\varphi_{br}\varphi_{pb} + a_{114}\varphi_{br}\theta_{mp}$$
$$+ a_{115}\theta_{br}\psi_{br} + a_{116}\theta_{br}\varphi_{pb} + a_{117}\theta_{br}\theta_{mp} + a_{118}\psi_{br}\varphi_{pb}$$
$$+ a_{119}\psi_{br}\theta_{mp} + a_{120}\varphi_{pb}\theta_{mp}$$

$$\psi_{sm} = a_{201}\varphi_{br} + a_{202}\theta_{br} + a_{203}\psi_{br} + a_{204}\varphi_{pb} + a_{205}\theta_{mp} + a_{206}\frac{1}{2}\varphi_{br}^2$$
$$+ a_{207}\frac{1}{2}\theta_{br}^2 + a_{208}\frac{1}{2}\psi_{br}^2 + a_{209}\frac{1}{2}\varphi_{pb}^2 + a_{210}\frac{1}{2}\theta_{mp}^2$$
$$+ a_{211}\varphi_{br}\theta_{br} + a_{212}\varphi_{br}\psi_{br} + a_{213}\varphi_{br}\varphi_{pb} + a_{214}\varphi_{br}\theta_{mp}$$
$$+ a_{215}\theta_{br}\psi_{br} + a_{216}\theta_{br}\varphi_{pb} + a_{217}\theta_{br}\theta_{mp} + a_{218}\psi_{br}\varphi_{pb}$$
$$+ a_{219}\psi_{br}\theta_{mp} + a_{220}\varphi_{pb}\theta_{mp}$$

$$\varphi_{sm} = a_{301}\varphi_{br} + a_{302}\theta_{br} + a_{303}\psi_{br} + a_{304}\varphi_{pb} + a_{305}\theta_{mp} + a_{306}\frac{1}{2}\varphi_{br}^2$$
$$+ a_{307}\frac{1}{2}\theta_{br}^2 + a_{308}\frac{1}{2}\psi_{br}^2 + a_{309}\frac{1}{2}\varphi_{pb}^2 + a_{310}\frac{1}{2}\theta_{mp}^2$$
$$+ a_{311}\varphi_{br}\theta_{br} + a_{312}\varphi_{br}\psi_{br} + a_{313}\varphi_{br}\varphi_{pb} + a_{314}\varphi_{br}\theta_{mp}$$
$$+ a_{315}\theta_{br}\psi_{br} + a_{316}\theta_{br}\varphi_{pb} + a_{317}\theta_{br}\theta_{mp} + a_{318}\psi_{br}\varphi_{pb}$$
$$+ a_{319}\psi_{br}\theta_{mp} + a_{320}\varphi_{pb}\theta_{mp}$$

$$-\theta_{tp} = a_{401}\varphi_{br} + a_{402}\theta_{br} + a_{403}\psi_{br} + a_{404}\varphi_{pb} + a_{405}\theta_{mp} + a_{406}\frac{1}{2}\varphi_{br}^2$$
$$+ a_{407}\frac{1}{2}\theta_{br}^2 + a_{408}\frac{1}{2}\psi_{br}^2 + a_{409}\frac{1}{2}\varphi_{pb}^2 + a_{410}\frac{1}{2}\theta_{mp}^2 + a_{411}\varphi_{br}\theta_{br}$$
$$+ a_{412}\varphi_{br}\psi_{br} + a_{413}\varphi_{br}\varphi_{pb} + a_{414}\varphi_{br}\theta_{mp} + a_{415}\theta_{br}\psi_{br} + a_{416}\theta_{br}\varphi_{pb}$$
$$+ a_{417}\theta_{br}\theta_{mp} + a_{418}\psi_{br}\varphi_{pb} + a_{419}\psi_{br}\theta_{mp} + a_{420}\varphi_{pb}\theta_{mp} + a_{421}\psi_{tP}$$
$$+ a_{422}\theta_{tP} + a_{423}\varphi_{tP} + a_{424}\frac{1}{2}\psi_{tP}^2 + a_{425}\frac{1}{2}\theta_{tP}^2 + a_{426}\frac{1}{2}\varphi_{tP}^2$$
$$+ a_{427}\varphi_{tP}\theta_{tP} + a_{428}\varphi_{tP}\psi_{tP} + a_{429}\theta_{tP}\psi_{tP} + a_{430}\varphi_{bP}\psi_{tP}$$
$$+ a_{431}\varphi_{bP}\theta_{tP} + a_{432}\varphi_{br}\varphi_{tP} + a_{433}\theta_{br}\psi_{tP} + a_{434}\theta_{br}\theta_{tP} + a_{435}\theta_{br}\varphi_{tP}$$
$$+ a_{436}\psi_{br}\psi_{tP} + a_{437}\psi_{br}\theta_{tP} + a_{438}\psi_{br}\varphi_{tP} + a_{439}\varphi_{pb}\psi_{tP} + a_{440}\varphi_{pb}\theta_{tP}$$
$$+ a_{441}\varphi_{pb}\varphi_{tP}$$

$$\psi_{tp} = a_{501}\varphi_{br} + a_{502}\theta_{br} + a_{503}\psi_{br} + a_{504}\varphi_{pb} + a_{505}\theta_{mp} + a_{506}\frac{1}{2}\varphi_{br}^2$$
$$+ a_{507}\frac{1}{2}\theta_{br}^2 + a_{508}\frac{1}{2}\psi_{br}^2 + a_{509}\frac{1}{2}\varphi_{pb}^2 + a_{510}\frac{1}{2}\theta_{mp}^2 + a_{511}\varphi_{br}\theta_{br}$$
$$+ a_{512}\varphi_{br}\psi_{br} + a_{513}\varphi_{br}\varphi_{pb} + a_{514}\varphi_{br}\theta_{mp} + a_{515}\theta_{br}\psi_{br} + a_{516}\theta_{br}\varphi_{pb}$$
$$+ a_{517}\theta_{br}\theta_{mp} + a_{518}\psi_{br}\varphi_{pb} + a_{519}\psi_{br}\theta_{mp} + a_{520}\varphi_{pb}\theta_{mp} + a_{521}\psi_{tP} + a_{522}\theta_{tP}$$
$$+ a_{523}\varphi_{tP} + a_{524}\frac{1}{2}\psi_{tP}^2 + a_{525}\frac{1}{2}\theta_{tP}^2 + a_{526}\frac{1}{2}\varphi_{tP}^2 + a_{527}\varphi_{tP}\theta_{tP}$$
$$+ a_{528}\varphi_{tP}\psi_{tP} + a_{529}\theta_{tP}\psi_{tP} + a_{530}\varphi_{br}\psi_{tP} + a_{531}\varphi_{br}\theta_{tP} + a_{532}\varphi_{br}\varphi_{tP}$$
$$+ a_{533}\theta_{br}\psi_{tP} + a_{534}\theta_{br}\theta_{tP} + a_{535}\theta_{br}\varphi_{tP} + a_{536}\psi_{br}\psi_{tP} + a_{537}\psi_{br}\theta_{tP}$$
$$+ a_{538}\psi_{br}\varphi_{tP} + a_{539}\varphi_{pb}\psi_{tP} + a_{540}\varphi_{pb}\theta_{tP} + a_{541}\varphi_{pb}\varphi_{tP}$$

$$\varphi_{tp} = a_{601}\varphi_{br} + a_{602}\theta_{br} + a_{603}\psi_{br}\, a_{604}\varphi_{pb} + a_{605}\theta_{mp} + a_{606}\frac{1}{2}\varphi_{br}^2 + a_{607}\frac{1}{2}\theta_{br}^2$$

$$+ a_{608}\frac{1}{2}\psi_{br}^2 + a_{609}\frac{1}{2}\varphi_{pb}^2 + a_{610}\frac{1}{2}\theta_{mp}^2 + a_{611}\varphi_{br}\theta_{br} + a_{612}\varphi_{br}\psi_{br}$$

$$+ a_{613}\varphi_{br}\varphi_{pb} + a_{614}\varphi_{br}\theta_{mp} + a_{615}\theta_{br}\psi_{br} + a_{616}\theta_{br}\varphi_{pb} + a_{617}\theta_{br}\theta_{mp}$$

$$+ a_{618}\psi_{br}\varphi_{pb} + a_{619}\psi_{br}\theta_{mp} + a_{620}\varphi_{pb}\theta_{mp} + a_{621}\psi_{tP} + a_{622}\theta_{tP} + a_{623}\varphi_{tP}$$

$$+ a_{624}\frac{1}{2}\psi_{tP}^2 + a_{625}\frac{1}{2}\theta_{tP}^2 + a_{626}\frac{1}{2}\varphi_{tP}^2 + a_{627}\varphi_{tP}\theta_{tP} + a_{628}\varphi_{tP}\psi_{tP}$$

$$+ a_{629}\theta_{tP}\psi_{tP} + a_{630}\varphi_{br}\psi_{tP} + a_{631}\varphi_{br}\theta_{tP} + a_{632}\varphi_{br}\varphi_{tP} + a_{633}\theta_{bR}\psi_{tP}$$

$$+ a_{634}\theta_{br}\theta_{tP} + a_{635}\theta_{br}\varphi_{tP} + a_{636}\psi_{br}\psi_{tP} + a_{637}\psi_{br}\theta_{tP} + a_{638}\psi_{br}\varphi_{tP}$$

$$+ a_{639}\varphi_{pb}\psi_{tP} + a_{640}\varphi_{pb}\theta_{tP} + a_{641}\varphi_{pb}\varphi_{tP}$$

Error Readout

$$\theta_{st} = -\theta_{tP} + \psi_{tP}^2\left(\frac{1}{2}\tan\Theta_{mp}\right)$$

$$\text{Error} = \theta_{mp} - \theta_{st}$$

MATRIX EQUATIONS FOR COEFFICIENTS

Display Angle Coefficients

Large angle matrices.-

$$M_{MP} = M_{MP}(\Theta_{mp}) = \begin{bmatrix} \cos\Theta & 0 & -\sin\Theta \\ 0 & 1 & 0 \\ \sin\Theta & 0 & \cos\Theta \end{bmatrix}_{MP}$$

$$M_{MP}^{-1} = \begin{bmatrix} \cos \Theta & 0 & \sin \Theta \\ 0 & 1 & 0 \\ -\sin \Theta & 0 & \cos \Theta \end{bmatrix}_{MP}$$

$$M_{PB} = M_{PB}(\Theta_{pb}, \Phi_{pb})$$

$$= \begin{bmatrix} \cos \Theta & 0 & -\sin \Theta \\ \sin \Theta \sin \Phi & \cos \Phi & \cos \Theta \sin \Phi \\ \sin \Theta \cos \Phi & -\sin \Phi & \cos \Theta \cos \Phi \end{bmatrix}_{PB}$$

$$M_{PB}^{-1} = \begin{bmatrix} \cos \Theta & \sin \Theta \sin \Phi & \sin \Theta \cos \Phi \\ 0 & \cos \Phi & -\sin \Phi \\ -\sin \Theta & \cos \Theta \sin \Phi & \cos \Theta \cos \Phi \end{bmatrix}_{PB}$$

$$M_{MB} = M_{MP} M_{PB}$$

$$M_{MB}^{-1} = M_{PB}^{-1} M_{MP}^{-1}$$

Coefficient matrices for star angles.-

	Variable	Coefficients	Coefficient matrix equations
1)	φ_{br}	$\begin{bmatrix} - & - & - \\ a_{201} & - & - \\ a_{101} & a_{301} & - \end{bmatrix}$	$= M_{MB} \begin{bmatrix} 0 & 0 & 0 \\ 0 & 0 & 1 \\ 0 & -1 & 0 \end{bmatrix} M_{MB}^{-1}$
2)	θ_{br}	$\begin{bmatrix} - & - & - \\ a_{202} & - & - \\ a_{102} & a_{302} & - \end{bmatrix}$	$= M_{MB} \begin{bmatrix} 0 & 0 & -1 \\ 0 & 0 & 0 \\ 1 & 0 & 0 \end{bmatrix} M_{MB}^{-1}$

	Variable	Coefficients		Coefficient matrix equations
3)	ψ_{br}	$\begin{bmatrix} - & - & - \\ a_{203} & - & - \\ a_{103} & a_{303} & - \end{bmatrix}$	$= M_{MB}$	$\begin{bmatrix} 0 & 1 & 0 \\ -1 & 0 & 0 \\ 0 & 0 & 0 \end{bmatrix} M_{MB}^{-1}$
4)	φ_{pb}	$\begin{bmatrix} - & - & - \\ a_{204} & - & - \\ a_{104} & a_{304} & - \end{bmatrix}$	$= M_{MP}$	$\begin{bmatrix} 0 & 0 & 0 \\ 0 & 0 & 1 \\ 0 & -1 & 0 \end{bmatrix} M_{MP}^{-1}$
5)	θ_{mp}	$\begin{bmatrix} - & - & - \\ a_{205} & - & - \\ a_{105} & a_{305} & - \end{bmatrix}$	$=$	$\begin{bmatrix} 0 & 0 & -1 \\ 0 & 0 & 0 \\ 1 & 0 & 0 \end{bmatrix}$
6)	$\frac{1}{2}\varphi_{br}^2$	$\begin{bmatrix} - & - & - \\ a_{206} & - & - \\ a_{106} & a_{306} & - \end{bmatrix}$	$= M_{MB}$	$\begin{bmatrix} 0 & 0 & 0 \\ 0 & -1 & 0 \\ 0 & 0 & -1 \end{bmatrix} M_{MB}^{-1}$
7)	$\frac{1}{2}\theta_{br}^2$	$\begin{bmatrix} - & - & - \\ a_{207} & - & - \\ a_{107} & a_{307} & - \end{bmatrix}$	$= M_{MB}$	$\begin{bmatrix} -1 & 0 & 0 \\ 0 & 0 & 0 \\ 0 & 0 & -1 \end{bmatrix} M_{MB}^{-1}$
8)	$\frac{1}{2}\psi_{br}^2$	$\begin{bmatrix} - & - & - \\ a_{208} & - & - \\ a_{108} & a_{308} & - \end{bmatrix}$	$= M_{MB}$	$\begin{bmatrix} -1 & 0 & 0 \\ 0 & -1 & 0 \\ 0 & 0 & 0 \end{bmatrix} M_{MB}^{-1}$
9)	$\frac{1}{2}\varphi_{pb}^2$	$\begin{bmatrix} - & - & - \\ a_{209} & - & - \\ a_{109} & a_{309} & - \end{bmatrix}$	$= M_{MP}$	$\begin{bmatrix} 0 & 0 & 0 \\ 0 & -1 & 0 \\ 0 & 0 & -1 \end{bmatrix} M_{MP}^{-1}$

	Variable	Coefficients		Coefficient matrix equations
10)	$\frac{1}{2}\theta_{mp}^2$	$\begin{bmatrix} - & - & - \\ a_{210} & - & - \\ a_{110} & a_{310} & - \end{bmatrix}$	$=$	$\begin{bmatrix} -1 & 0 & 0 \\ 0 & 0 & 0 \\ 0 & 0 & -1 \end{bmatrix}$
11)	$\varphi_{br}\theta_{br}$	$\begin{bmatrix} - & - & - \\ a_{211} & - & - \\ a_{111} & a_{311} & - \end{bmatrix}$	$= M_{MB}$	$\begin{bmatrix} 0 & 0 & 0 \\ 1 & 0 & 0 \\ 0 & 0 & 0 \end{bmatrix} M_{MB}^{-1}$
12)	$\varphi_{br}\psi_{br}$	$\begin{bmatrix} - & - & - \\ a_{212} & - & - \\ a_{112} & a_{312} & - \end{bmatrix}$	$= M_{MB}$	$\begin{bmatrix} 0 & 0 & 0 \\ 0 & 0 & 0 \\ 1 & 0 & 0 \end{bmatrix} M_{MB}^{-1}$
13)	$\varphi_{br}\varphi_{pb}$	$\begin{bmatrix} - & - & - \\ a_{213} & - & - \\ a_{113} & a_{313} & - \end{bmatrix}$	$= \left\{ M_{MP} \begin{bmatrix} 0 & 0 & 0 \\ 0 & 0 & 1 \\ 0 & -1 & 0 \end{bmatrix} M_{MP}^{-1} \right\} \left\{ M_{MB} \begin{bmatrix} 0 & 0 & 0 \\ 0 & 0 & 1 \\ 0 & -1 & 0 \end{bmatrix} M_{MB}^{-1} \right\}$	
14)	$\varphi_{br}\theta_{mp}$	$\begin{bmatrix} - & - & - \\ a_{214} & - & - \\ a_{114} & a_{314} & - \end{bmatrix}$	$=$	$\begin{bmatrix} 0 & 0 & -1 \\ 0 & 0 & 0 \\ 1 & 0 & 0 \end{bmatrix} \left\{ M_{MB} \begin{bmatrix} 0 & 0 & 0 \\ 0 & 0 & 1 \\ 0 & -1 & 0 \end{bmatrix} M_{MB}^{-1} \right\}$
15)	$\theta_{br}\psi_{br}$	$\begin{bmatrix} - & - & - \\ a_{215} & - & - \\ a_{115} & a_{315} & - \end{bmatrix}$	$= M_{MB}$	$\begin{bmatrix} 0 & 0 & 0 \\ 0 & 0 & 0 \\ 0 & 1 & 0 \end{bmatrix} M_{MB}^{-1}$
16)	$\theta_{br}\varphi_{pb}$	$\begin{bmatrix} - & - & - \\ a_{216} & - & - \\ a_{116} & a_{316} & - \end{bmatrix}$	$= \left\{ M_{MP} \begin{bmatrix} 0 & 0 & 0 \\ 0 & 0 & 1 \\ 0 & -1 & 0 \end{bmatrix} M_{MP}^{-1} \right\} \left\{ M_{MB} \begin{bmatrix} 0 & 0 & -1 \\ 0 & 0 & 0 \\ 1 & 0 & 0 \end{bmatrix} M_{MB}^{-1} \right\}$	

	Variable	Coefficients	Coefficient matrix equations

17) $\theta_{br}\theta_{mp}$

$$\begin{bmatrix} - & - & - \\ a_{217} & - & - \\ a_{117} & a_{317} & - \end{bmatrix} = \begin{bmatrix} 0 & 0 & -1 \\ 0 & 0 & 0 \\ 1 & 0 & 0 \end{bmatrix} \left\{ M_{MB} \begin{bmatrix} 0 & 0 & -1 \\ 0 & 0 & 0 \\ 1 & 0 & 0 \end{bmatrix} M_{MB}^{-1} \right\}$$

18) $\psi_{br}\varphi_{pb}$

$$\begin{bmatrix} - & - & - \\ a_{218} & - & - \\ a_{118} & a_{318} & - \end{bmatrix} = \left\{ M_{MP} \begin{bmatrix} 0 & 0 & 0 \\ 0 & 0 & 1 \\ 0 & -1 & 0 \end{bmatrix} M_{MP}^{-1} \right\} \left\{ M_{MB} \begin{bmatrix} 0 & 1 & 0 \\ -1 & 0 & 0 \\ 0 & 0 & 0 \end{bmatrix} M_{MB}^{-1} \right\}$$

19) $\psi_{br}\theta_{mp}$

$$\begin{bmatrix} - & - & - \\ a_{219} & - & - \\ a_{119} & a_{319} & - \end{bmatrix} = \begin{bmatrix} 0 & 0 & -1 \\ 0 & 0 & 0 \\ 1 & 0 & 0 \end{bmatrix} \left\{ M_{MB} \begin{bmatrix} 0 & 1 & 0 \\ -1 & 0 & 0 \\ 0 & 0 & 0 \end{bmatrix} M_{MB}^{-1} \right\}$$

20) $\varphi_{pb}\theta_{mp}$

$$\begin{bmatrix} - & - & - \\ a_{220} & - & - \\ a_{120} & a_{320} & - \end{bmatrix} = \begin{bmatrix} 0 & 0 & -1 \\ 0 & 0 & 0 \\ 1 & 0 & 0 \end{bmatrix} \left\{ M_{MP} \begin{bmatrix} 0 & 0 & 0 \\ 0 & 0 & 1 \\ 0 & -1 & 0 \end{bmatrix} M_{MP}^{-1} \right\}$$

Coefficient matrices for landmark angles.-

	Variable	Coefficients	Coefficient matrix equations

1) φ_{br}

$$\begin{bmatrix} - & - & - \\ a_{501} & - & - \\ a_{401} & a_{601} & - \end{bmatrix} = M_{PB} \begin{bmatrix} 0 & 0 & 0 \\ 0 & 0 & 1 \\ 0 & -1 & 0 \end{bmatrix} M_{PB}^{-1}$$

2) θ_{br}

$$\begin{bmatrix} - & - & - \\ a_{502} & - & - \\ a_{402} & a_{602} & - \end{bmatrix} = M_{PB} \begin{bmatrix} 0 & 0 & -1 \\ 0 & 0 & 0 \\ 1 & 0 & 0 \end{bmatrix} M_{PB}^{-1}$$

	Variable	Coefficients	Coefficient matrix equations
3)	ψ_{br}	$\begin{bmatrix} - & - & - \\ a_{503} & - & - \\ a_{403} & a_{603} & - \end{bmatrix}$	$= M_{PB} \begin{bmatrix} 0 & 1 & 0 \\ -1 & 0 & 0 \\ 0 & 0 & 0 \end{bmatrix} M_{PB}^{-1}$
4)	φ_{pb}	$\begin{bmatrix} - & - & - \\ a_{504} & - & - \\ a_{404} & a_{604} & - \end{bmatrix}$	$= \begin{bmatrix} 0 & 0 & 0 \\ 0 & 0 & 1 \\ 0 & -1 & 0 \end{bmatrix}$
5)	θ_{mp}		0
6)	$\frac{1}{2}\varphi_{br}^2$	$\begin{bmatrix} - & - & - \\ a_{506} & - & - \\ a_{406} & a_{606} & - \end{bmatrix}$	$= M_{PB} \begin{bmatrix} 0 & 0 & 0 \\ 0 & -1 & 0 \\ 0 & 0 & -1 \end{bmatrix} M_{PB}^{-1}$
7)	$\frac{1}{2}\theta_{br}^2$	$\begin{bmatrix} - & - & - \\ a_{507} & - & - \\ a_{407} & a_{607} & - \end{bmatrix}$	$= M_{PB} \begin{bmatrix} -1 & 0 & 0 \\ 0 & 0 & 0 \\ 0 & 0 & -1 \end{bmatrix} M_{PB}^{-1}$
8)	$\frac{1}{2}\psi_{br}^2$	$\begin{bmatrix} - & - & - \\ a_{508} & - & - \\ a_{408} & a_{608} & - \end{bmatrix}$	$= M_{PB} \begin{bmatrix} -1 & 0 & 0 \\ 0 & -1 & 0 \\ 0 & 0 & 0 \end{bmatrix} M_{PB}^{-1}$
9)	$\frac{1}{2}\varphi_{pb}^2$	$\begin{bmatrix} - & - & - \\ a_{509} & - & - \\ a_{409} & a_{609} & - \end{bmatrix}$	$= \begin{bmatrix} 0 & 0 & 0 \\ 0 & -1 & 0 \\ 0 & 0 & -1 \end{bmatrix}$

	Variable	Coefficients	Coefficient matrix equations
10)	$\frac{1}{2}\theta_{mp}^2$		0
11)	$\varphi_{br}\theta_{br}$	$\begin{bmatrix} - & - & - \\ a_{511} & - & - \\ a_{411} & a_{611} & - \end{bmatrix}$	$= M_{PB}\begin{bmatrix} 0 & 0 & 0 \\ 1 & 0 & 0 \\ 0 & 0 & 0 \end{bmatrix} M_{PB}^{-1}$
12)	$\varphi_{br}\psi_{br}$	$\begin{bmatrix} - & - & - \\ a_{512} & - & - \\ a_{412} & a_{612} & - \end{bmatrix}$	$= M_{PB}\begin{bmatrix} 0 & 0 & 0 \\ 0 & 0 & 0 \\ 1 & 0 & 0 \end{bmatrix} M_{PB}^{-i}$
13)	$\varphi_{br}\varphi_{pb}$	$\begin{bmatrix} - & - & - \\ a_{513} & - & - \\ a_{413} & a_{613} & - \end{bmatrix}$	$= \begin{bmatrix} 0 & 0 & 0 \\ 0 & 0 & 1 \\ 0 & -1 & 0 \end{bmatrix} \left\{ M_{PB}\begin{bmatrix} 0 & 0 & 0 \\ 0 & 0 & 1 \\ 0 & -1 & 0 \end{bmatrix} M_{PB}^{-1} \right\}$
14)	$\varphi_{br}\theta_{mp}$		0
15)	$\theta_{br}\psi_{br}$	$\begin{bmatrix} - & - & - \\ a_{515} & - & - \\ a_{415} & a_{615} & - \end{bmatrix}$	$= M_{PB}\begin{bmatrix} 0 & 0 & 0 \\ 0 & 0 & 0 \\ 0 & 1 & 0 \end{bmatrix} M_{PB}^{-1}$
16)	$\theta_{br}\varphi_{pb}$	$\begin{bmatrix} - & - & - \\ a_{516} & - & - \\ a_{416} & a_{616} & - \end{bmatrix}$	$= \begin{bmatrix} 0 & 0 & 0 \\ 0 & 0 & 1 \\ 0 & -1 & 0 \end{bmatrix} \left\{ M_{PB}\begin{bmatrix} 0 & 0 & -1 \\ 0 & 0 & 0 \\ 1 & 0 & 0 \end{bmatrix} M_{PB}^{-1} \right\}$
17)	$\theta_{br}\theta_{mp}$		0

	Variable	Coefficients	Coefficient matrix equations
18)	$\psi_{br}\varphi_{pb}$	$\begin{bmatrix} - & - & - \\ a_{518} & - & - \\ a_{418} & a_{618} & - \end{bmatrix}$	$= \begin{bmatrix} 0 & 0 & 0 \\ 0 & 0 & 1 \\ 0 & -1 & 0 \end{bmatrix} \left\{ M_{PB} \begin{bmatrix} 0 & 1 & 0 \\ -1 & 0 & 0 \\ 0 & 0 & 0 \end{bmatrix} M_{PB}^{-1} \right\}$
19)	$\psi_{br}\theta_{mp}$		0
20)	$\varphi_{pb}\theta_{mp}$		0
21)	ψ_{tP}	$\begin{bmatrix} - & - & - \\ a_{521} & - & - \\ a_{421} & a_{621} & - \end{bmatrix}$	$= \begin{bmatrix} 0 & -1 & 0 \\ 1 & 0 & 0 \\ 0 & 0 & 0 \end{bmatrix}$
22)	θ_{tP}	$\begin{bmatrix} - & - & - \\ a_{522} & - & - \\ a_{422} & a_{622} & - \end{bmatrix}$	$= \begin{bmatrix} 0 & 0 & 1 \\ 0 & 0 & 0 \\ -1 & 0 & 0 \end{bmatrix}$
23)	φ_{tP}	$\begin{bmatrix} - & - & - \\ a_{523} & - & - \\ a_{423} & a_{623} & - \end{bmatrix}$	$= \begin{bmatrix} 0 & 0 & 0 \\ 0 & 0 & -1 \\ 0 & 1 & 0 \end{bmatrix}$
24)	$\frac{1}{2}\psi_{tP}^2$	$\begin{bmatrix} - & - & - \\ a_{524} & - & - \\ a_{424} & a_{624} & - \end{bmatrix}$	$= \begin{bmatrix} -1 & 0 & 0 \\ 0 & -1 & 0 \\ 0 & 0 & 0 \end{bmatrix}$
25)	$\frac{1}{2}\theta_{tP}^2$	$\begin{bmatrix} - & - & - \\ a_{525} & - & - \\ a_{425} & a_{625} & - \end{bmatrix}$	$= \begin{bmatrix} -1 & 0 & 0 \\ 0 & 0 & 0 \\ 0 & 0 & -1 \end{bmatrix}$
26)	$\frac{1}{2}\varphi_{tP}^2$	$\begin{bmatrix} - & - & - \\ a_{526} & - & - \\ a_{426} & a_{626} & - \end{bmatrix}$	$= \begin{bmatrix} 0 & 0 & 0 \\ 0 & -1 & 0 \\ 0 & 0 & -1 \end{bmatrix}$

	Variable	Coefficients	Coefficient matrix equations

27) $\varphi_{tP}\theta_{tP}$

$$\begin{bmatrix} - & - & - \\ a_{527} & - & - \\ a_{427} & a_{627} & - \end{bmatrix} = \begin{bmatrix} 0 & 1 & 0 \\ 0 & 0 & 0 \\ 0 & 0 & 0 \end{bmatrix}$$

28) $\varphi_{tP}\psi_{tP}$

$$\begin{bmatrix} - & - & - \\ a_{528} & - & - \\ a_{428} & a_{628} & - \end{bmatrix} = \begin{bmatrix} 0 & 0 & 1 \\ 0 & 0 & 0 \\ 0 & 0 & 0 \end{bmatrix}$$

29) $\theta_{tP}\psi_{tP}$

$$\begin{bmatrix} - & - & - \\ a_{529} & - & - \\ a_{429} & a_{629} & - \end{bmatrix} = \begin{bmatrix} 0 & 0 & 0 \\ 0 & 0 & 1 \\ 0 & 0 & 0 \end{bmatrix}$$

30) $\varphi_{br}\psi_{tP}$

$$\begin{bmatrix} - & - & - \\ a_{530} & - & - \\ a_{430} & a_{630} & - \end{bmatrix} = M_{PB} \begin{bmatrix} 0 & 0 & 0 \\ 0 & 0 & 1 \\ 0 & -1 & 0 \end{bmatrix} M_{PB}^{-1} \begin{bmatrix} 0 & -1 & 0 \\ 1 & 0 & 0 \\ 0 & 0 & 0 \end{bmatrix}$$

31) $\varphi_{br}\theta_{tP}$

$$\begin{bmatrix} - & - & - \\ a_{531} & - & - \\ a_{431} & a_{631} & - \end{bmatrix} = M_{PB} \begin{bmatrix} 0 & 0 & 0 \\ 0 & 0 & 1 \\ 0 & -1 & 0 \end{bmatrix} M_{PB}^{-1} \begin{bmatrix} 0 & 0 & 1 \\ 0 & 0 & 0 \\ -1 & 0 & 0 \end{bmatrix}$$

32) $\varphi_{br}\varphi_{tP}$

$$\begin{bmatrix} - & - & - \\ a_{532} & - & - \\ a_{432} & a_{632} & - \end{bmatrix} = M_{PB} \begin{bmatrix} 0 & 0 & 0 \\ 0 & 0 & 1 \\ 0 & -1 & 0 \end{bmatrix} M_{PB}^{-1} \begin{bmatrix} 0 & 0 & 0 \\ 0 & 0 & -1 \\ 0 & 1 & 0 \end{bmatrix}$$

33) $\theta_{br}\psi_{tP}$

$$\begin{bmatrix} - & - & - \\ a_{533} & - & - \\ a_{433} & a_{633} & - \end{bmatrix} = M_{PB} \begin{bmatrix} 0 & 0 & -1 \\ 0 & 0 & 0 \\ 1 & 0 & 0 \end{bmatrix} M_{PB}^{-1} \begin{bmatrix} 0 & -1 & 0 \\ 1 & 0 & 0 \\ 0 & 0 & 0 \end{bmatrix}$$

	Variable	Coefficients	Coefficient matrix equations
34)	$\theta_{br}\theta_{tP}$	$\begin{bmatrix} - & - & - \\ a_{534} & - & - \\ a_{434} & a_{634} & - \end{bmatrix}$	$= M_{PB} \begin{bmatrix} 0 & 0 & -1 \\ 0 & 0 & 0 \\ 1 & 0 & 0 \end{bmatrix} M_{PB}^{-1} \begin{bmatrix} 0 & 0 & 1 \\ 0 & 0 & 0 \\ -1 & 0 & 0 \end{bmatrix}$
35)	$\theta_{br}\varphi_{tP}$	$\begin{bmatrix} - & - & - \\ a_{535} & - & - \\ a_{435} & a_{635} & - \end{bmatrix}$	$= M_{PB} \begin{bmatrix} 0 & 0 & -1 \\ 0 & 0 & 0 \\ 1 & 0 & 0 \end{bmatrix} M_{PB}^{-1} \begin{bmatrix} 0 & 0 & 0 \\ 0 & 0 & -1 \\ 0 & 1 & 0 \end{bmatrix}$
36)	$\psi_{br}\psi_{tP}$	$\begin{bmatrix} - & - & - \\ a_{536} & - & - \\ a_{436} & a_{636} & - \end{bmatrix}$	$= M_{PB} \begin{bmatrix} 0 & 1 & 0 \\ -1 & 0 & 0 \\ 0 & 0 & 0 \end{bmatrix} M_{PB}^{-1} \begin{bmatrix} 0 & -1 & 0 \\ 1 & 0 & 0 \\ 0 & 0 & 0 \end{bmatrix}$
37)	$\psi_{br}\theta_{tP}$	$\begin{bmatrix} - & - & - \\ a_{537} & - & - \\ a_{437} & a_{637} & - \end{bmatrix}$	$= M_{PB} \begin{bmatrix} 0 & 1 & 0 \\ -1 & 0 & 0 \\ 0 & 0 & 0 \end{bmatrix} M_{PB}^{-1} \begin{bmatrix} 0 & 0 & 1 \\ 0 & 0 & 0 \\ -1 & 0 & 0 \end{bmatrix}$
38)	$\psi_{br}\varphi_{tP}$	$\begin{bmatrix} - & - & - \\ a_{538} & - & - \\ a_{438} & a_{638} & - \end{bmatrix}$	$= M_{PB} \begin{bmatrix} 0 & 1 & 0 \\ -1 & 0 & 0 \\ 0 & 0 & 0 \end{bmatrix} M_{PB}^{-1} \begin{bmatrix} 0 & 0 & 0 \\ 0 & 0 & -1 \\ 0 & 1 & 0 \end{bmatrix}$
39)	$\varphi_{pb}\psi_{tP}$	$\begin{bmatrix} - & - & - \\ a_{539} & - & - \\ a_{439} & a_{639} & - \end{bmatrix}$	$= \begin{bmatrix} 0 & 0 & 0 \\ 0 & 0 & 1 \\ 0 & -1 & 0 \end{bmatrix} \begin{bmatrix} 0 & -1 & 0 \\ 1 & 0 & 0 \\ 0 & 0 & 0 \end{bmatrix}$
40)	$\varphi_{pb}\theta_{tP}$	$\begin{bmatrix} - & - & - \\ a_{540} & - & - \\ a_{440} & a_{640} & - \end{bmatrix}$	$= \begin{bmatrix} 0 & 0 & 0 \\ 0 & 0 & 1 \\ 0 & -1 & 0 \end{bmatrix} \begin{bmatrix} 0 & 0 & 1 \\ 0 & 0 & 0 \\ -1 & 0 & 0 \end{bmatrix}$

	Variable	Coefficients	Coefficient matrix equations

41) $\varphi_{pb}\varphi_{tP}$

$$\begin{bmatrix} - & - & - \\ a_{541} & - & - \\ a_{441} & a_{641} & - \end{bmatrix} = \begin{bmatrix} 0 & 0 & 0 \\ 0 & 0 & 1 \\ 0 & -1 & 0 \end{bmatrix} \begin{bmatrix} 0 & 0 & 0 \\ 0 & 0 & -1 \\ 0 & 1 & 0 \end{bmatrix}$$

APPENDIX B

SEXTANT MEASUREMENT ERRORS DUE TO OFF-PLANE SIGHTINGS

A sextant's characteristics are such that the targets do not necessarily have to be superimposed or centered in the field of view in order to make an angle measurement. However errors do occur if the sextant plane of measurement is not coincident with the plane formed by the observer and the two targets. The mathematical model is used in the following development of the equation relating the actual angle between sighting objects and the measured sextant angle for off-plane sightings.

From figure 13,

$$M_{st} = M_{sr}M_{tr}^{-1}$$

$$M_{sr} = M_{sm}M_{mp}M_{pb}M_{br}$$

As before assume

$$M_{br} = I$$

and for this development assume

$$M_{pb} = I$$

then

$$M_{sr} = M_{sm}M_{mp}$$

Also

$$M_{tr} = M_{tp}M_{pb}M_{br}$$

but

$$M_{pb} = M_{br} = I$$

so

$$M_{tr} = M_{tp}$$

Therefore,

$$M_{st} = M_{sm} M_{mp} M_{tp}^{-1}$$

which can also be obtained by a direct three angle rotation,

$$M_{st}(\tilde{\Phi}_1, \tilde{\Theta}, \tilde{\Phi}_2)$$

Since the in-plane displacement of the images in the field of view can be any value, as long as both images are moved the same amount with respect to the principal "M" line, we will assume

$$\tilde{\Theta}_{sm} = \tilde{\Theta}_{tp} = 0$$

Then

$$M_{sm} = \begin{bmatrix} c\tilde{\Psi} & s\tilde{\Psi} & 0 \\ -s\tilde{\Psi} & c\tilde{\Psi} & 0 \\ 0 & 0 & 1 \end{bmatrix}$$

$$M_{sp} = \begin{bmatrix} c\tilde{\Theta} & 0 & -s\tilde{\Theta} \\ 0 & 1 & 0 \\ s\tilde{\Theta} & 0 & c\tilde{\Theta} \end{bmatrix}$$

$$M_{tp}^{-1} = \begin{bmatrix} c\tilde{\Psi} & -s\tilde{\Psi} & 0 \\ s\tilde{\Psi} & c\tilde{\Psi} & 0 \\ 0 & 0 & 1 \end{bmatrix}$$

Combining the above matrices we have

$$M_{st} = \begin{bmatrix} [c\tilde{\Psi}_{sm} c\tilde{\Theta}_{mp} c\tilde{\Psi}_{tp} + s\tilde{\Psi}_{sm} s\tilde{\Psi}_{tp}] & X & X \\ X & X & X \\ X & X & X \end{bmatrix} \qquad \text{(B1)}$$

Also, using the direct rotation $(\tilde{\Phi}_1,\tilde{\Theta},\tilde{\Phi}_2)$ we have

$$M_{st} = \begin{bmatrix} c\tilde{\Theta}_{st} & X & X \\ X & X & X \\ X & X & X \end{bmatrix} \tag{B2}$$

When elements k_{11} in (B1) and (B2) are equated

$$\cos \tilde{\Theta}_{st} = \cos \tilde{\Psi}_{sm} \cos \tilde{\Theta}_{mp} \cos \tilde{\Psi}_{tp} + \sin \tilde{\Psi}_{sm} \sin \tilde{\Psi}_{tp} \tag{B3}$$

where $\tilde{\Theta}_{st}$ is the true angle between sighting objects and $\tilde{\Theta}_{mp}$ is the sextant measured angle.

Equation (B3) was used to calculate the off-plane sighting measurement error $(\tilde{\Theta}_{st} - \tilde{\Theta}_{mp})$ for three cases:

I Landmark on plane, star off-plane, that is, $\tilde{\Psi}_{tp} = 0$ (fig. 19(a))

II Landmark and star superimposed off-plane, that is, $\tilde{\Psi}_{tp} = \tilde{\Psi}_{sm} \neq 0$ (fig. 19(b))

III Landmark and star on opposite sides of plane, that is, $\tilde{\Psi}_{tp} = -\tilde{\Psi}_{sm} \neq 0$ (fig. 19(c))

TABLE I.- SUMMARY OF PERFORMANCE OF NAVIGATOR-SEXTANT COMBINATION

[Initial large angles: Shaft roll 45°, Trunnion 45°]

	Base-line fixed vehicle attitude fixed landmark	No landmark motion; initial vehicle attitude motion[a]		Landmark motion; no initial vehicle attitude motion						Landmark motion plus vehicle attitude motion[a]		
		Controller inactive	Controller active[b]	Controller inactive (fixed vehicle)			Vehicle controller active[b]			Vehicle controller active[b]		
				Landmark rates[c]						Landmark rates[c]		
				28	280	560	28	280	560	28	280	560
3σ (arcsec)	6	9	6	6	21	39	6	10-1/2	21	8	10-1/2	12
av time (sec)	10-25	8	10-25	12	6	4	15	11	5	15	10	4
$\bar{N}_{yaw}$			0				0	0	0	3	2	2
$\bar{N}_{pitch}$			2				0	0	0	1	1	1
$\bar{N}_{roll}$			2				0	1	2	1	2	2

	Roll	Pitch	Yaw
[a]Vehicle attitude initial rates (arcsec/sec)	160	40	40
[b]Vehicle attitude controller rate per pulse (arcsec/sec per pulse)	320	80	80

[c]Resultant landmark line-of-sight rate for equal rates of in-plane and ortho-plane motion.

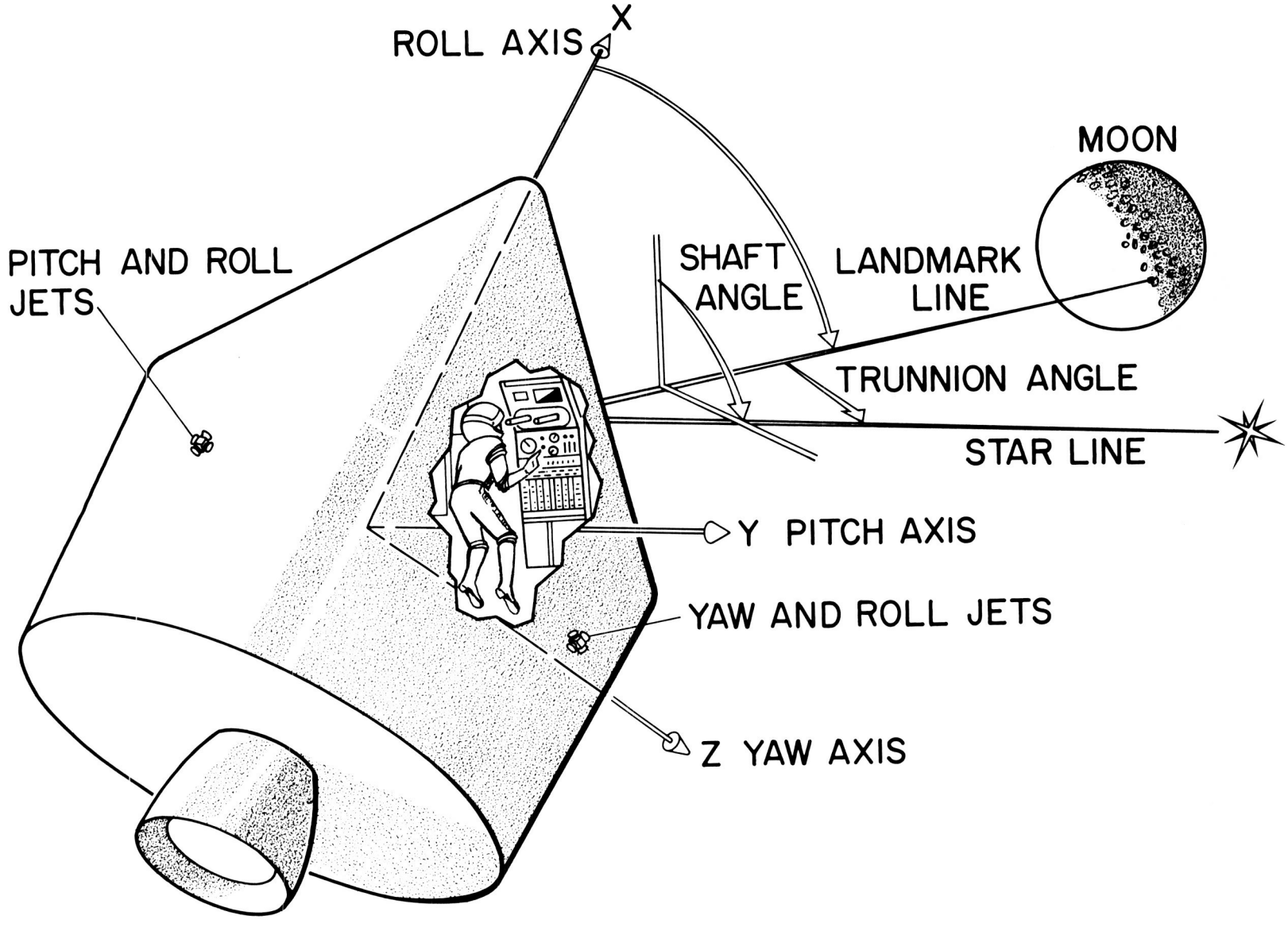

Figure 1.- Vehicle model.

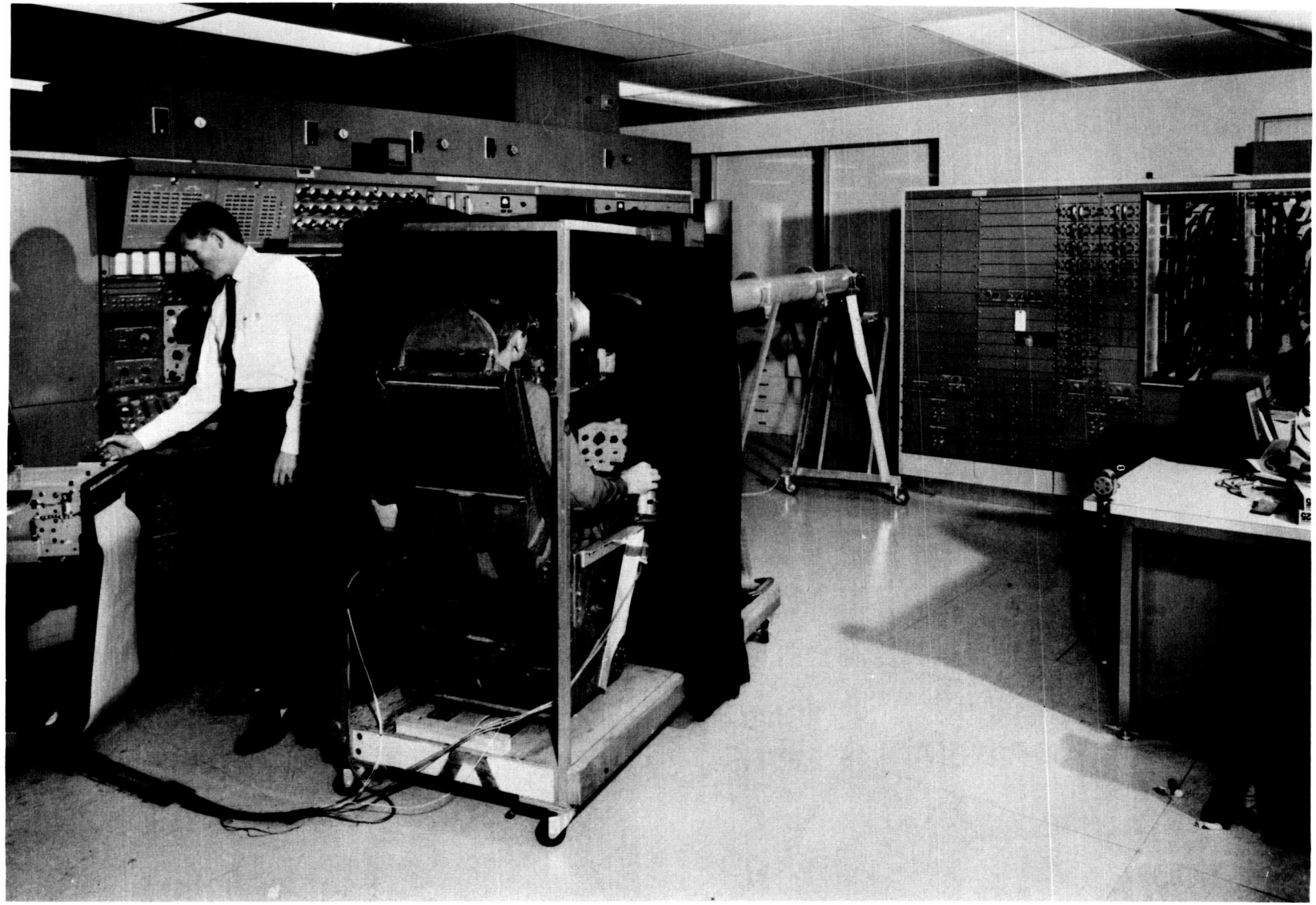

A-31877

Figure 2.- Sextant sighting simulator.

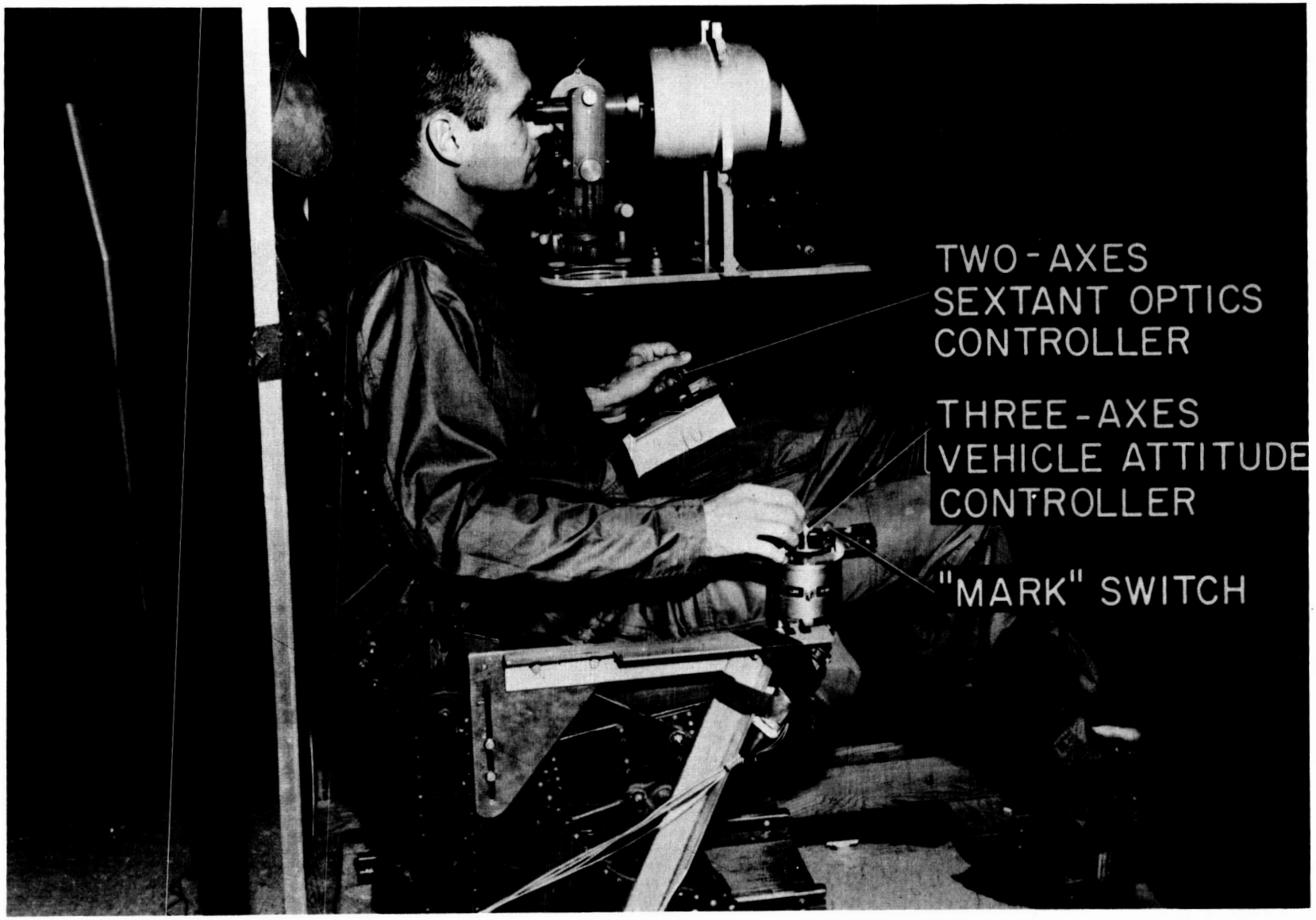

A-31879.1

Figure 3.- Simulated navigator's station.

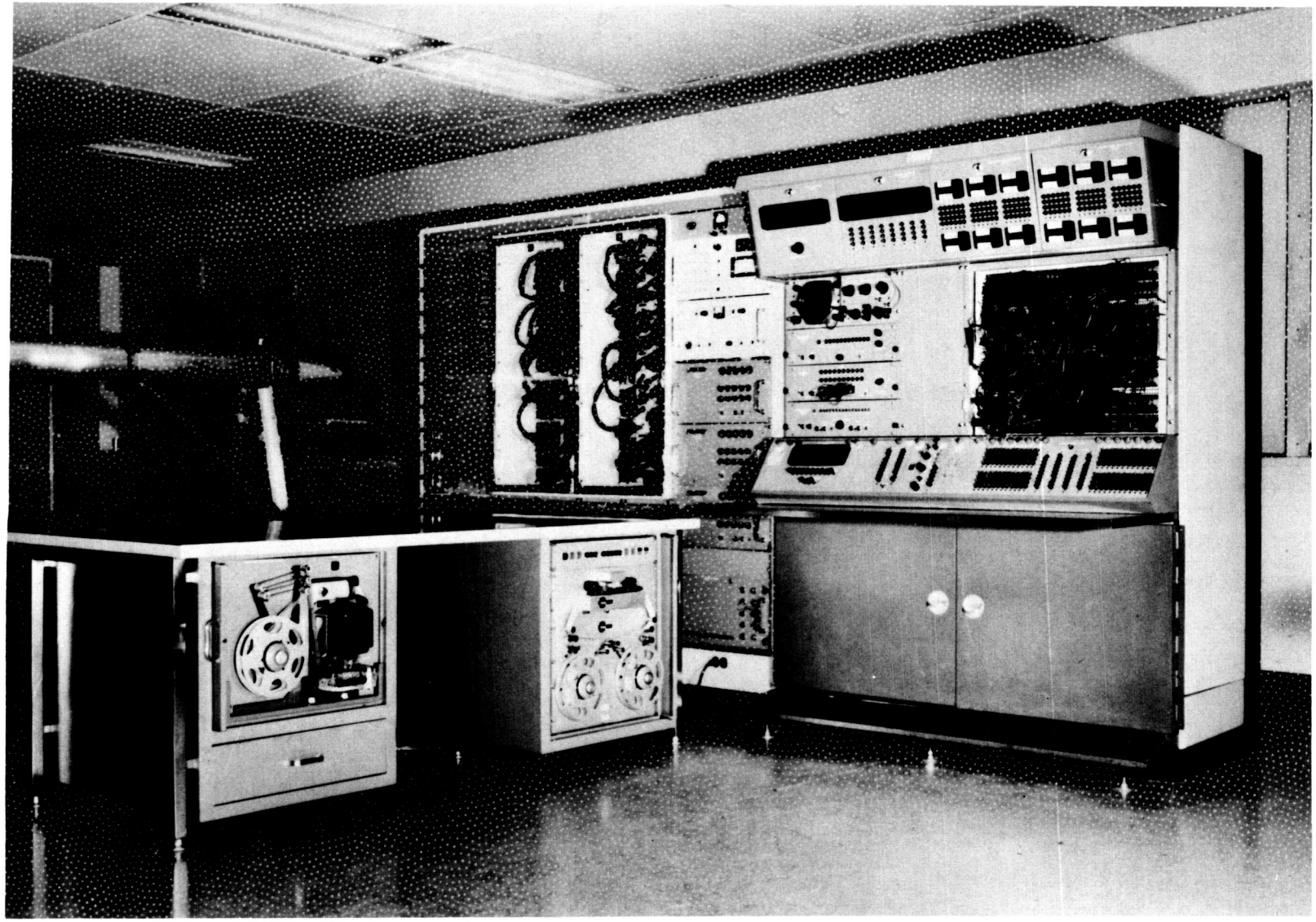

A-31108.1

Figure 4.- Digital logic simulator showing main console and input-output equipment desk.

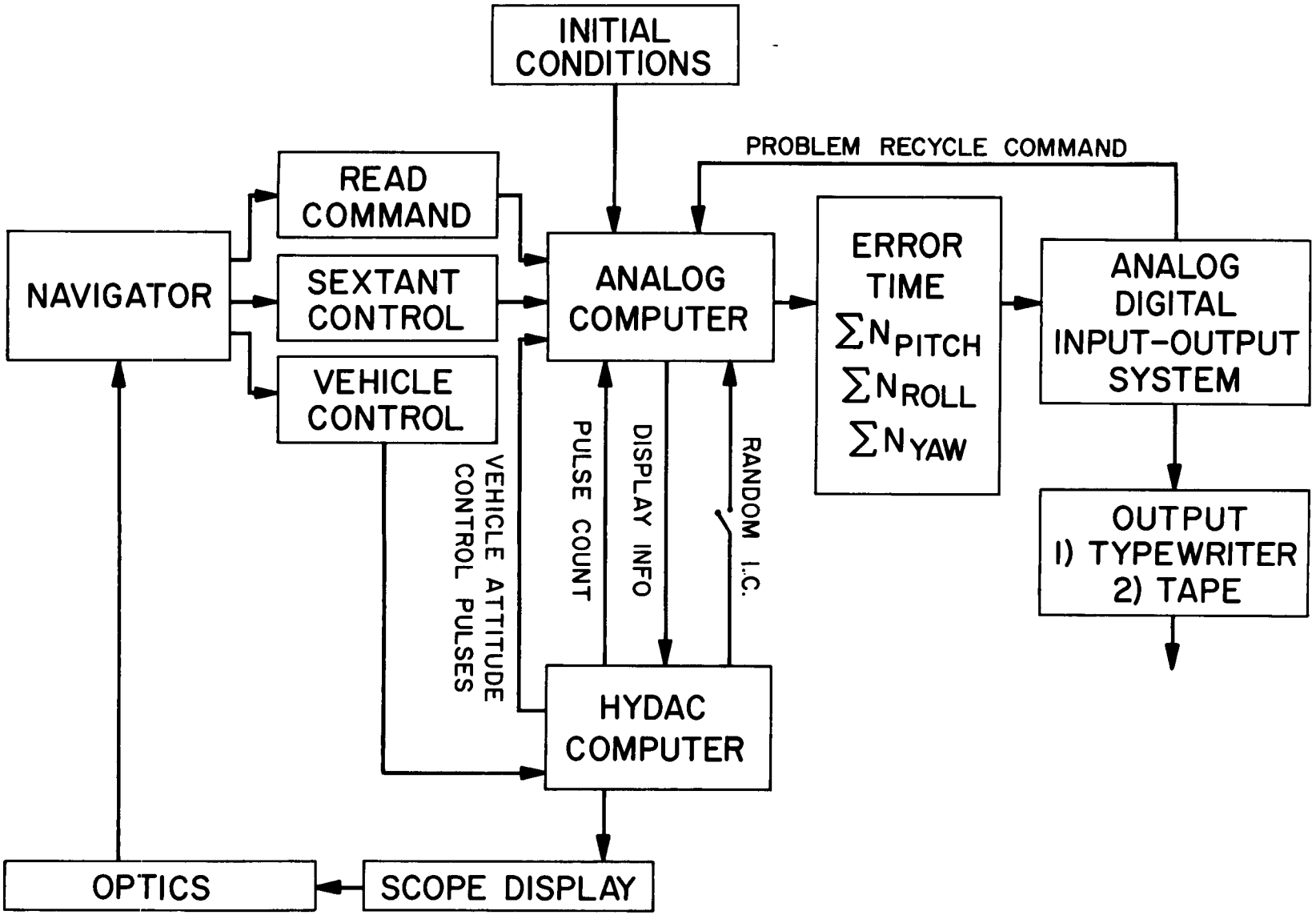

Figure 5.- Simulation information flow diagram.

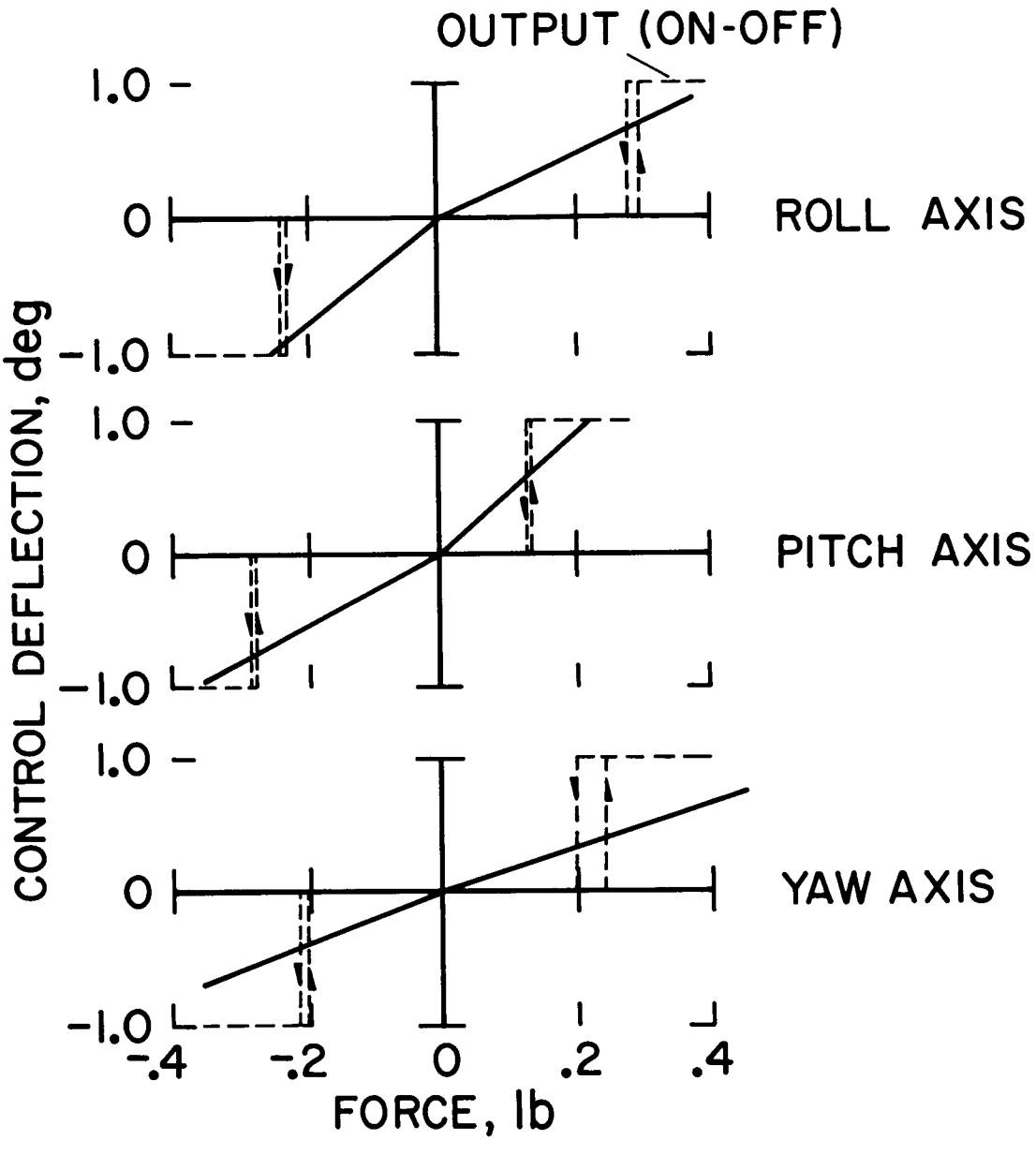

Figure 6.- Vehicle attitude controller characteristics.

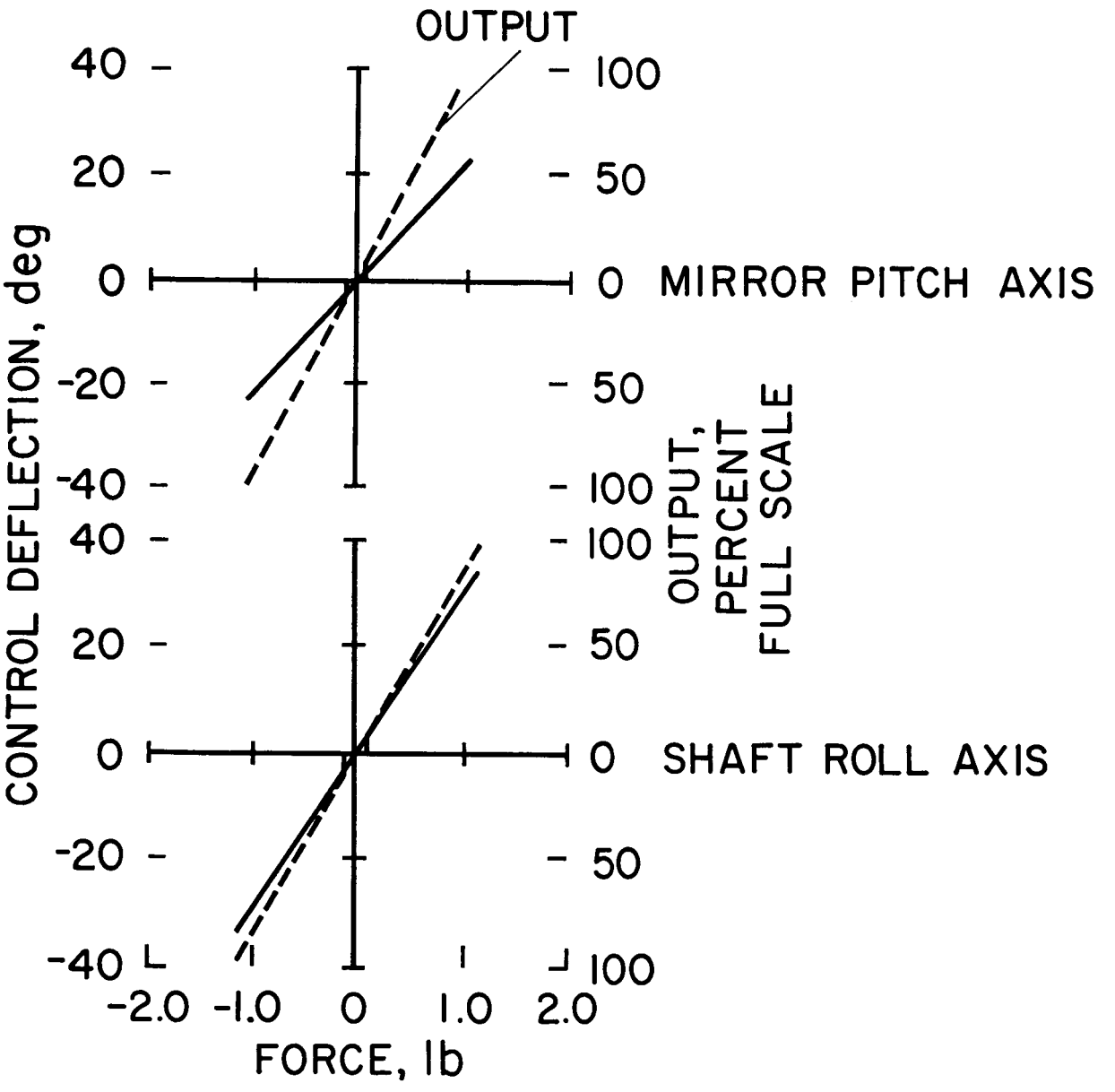

Figure 7.- Sextant optics controller characteristics.

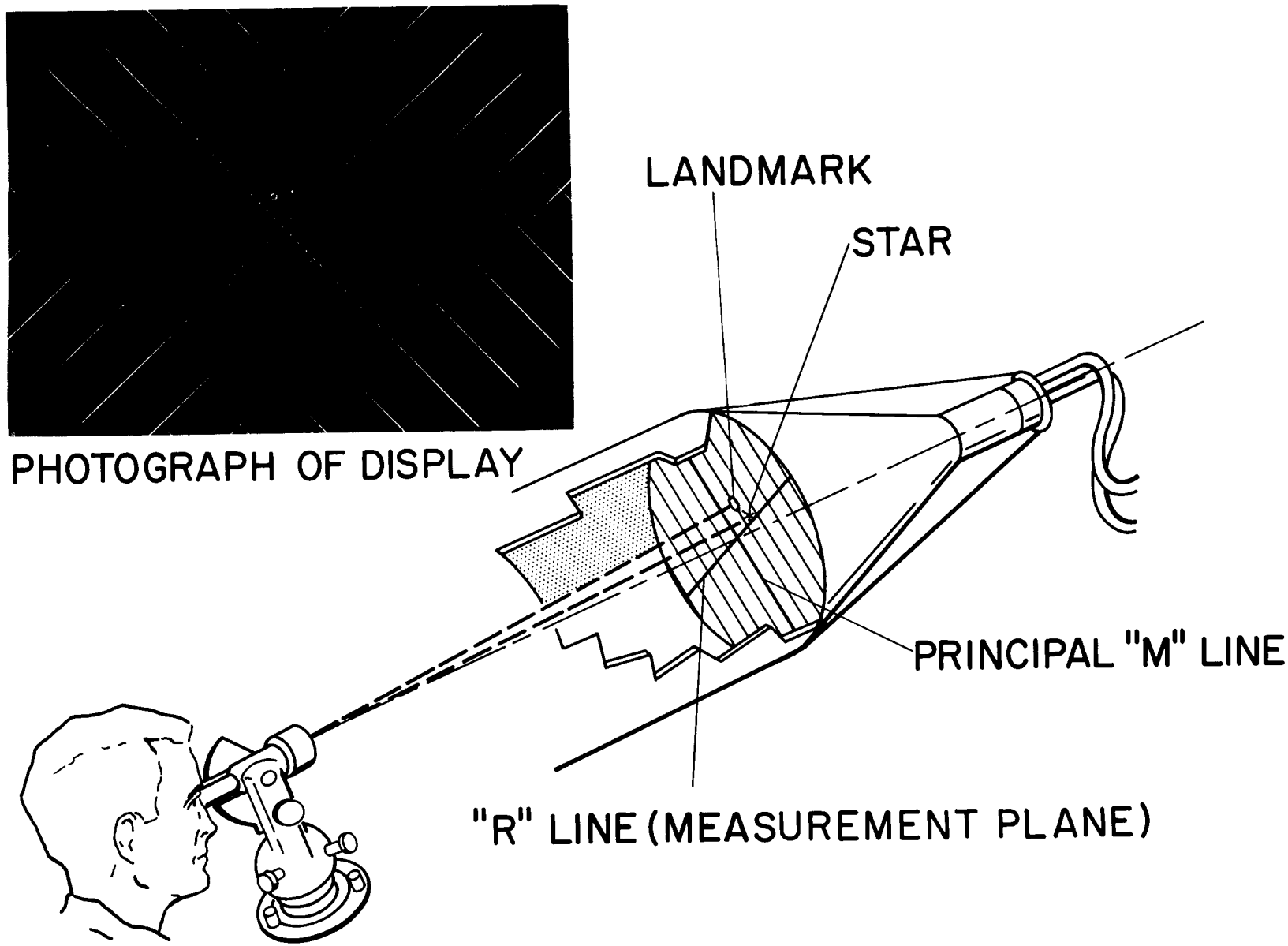

Figure 8.- Sextant simulation display.

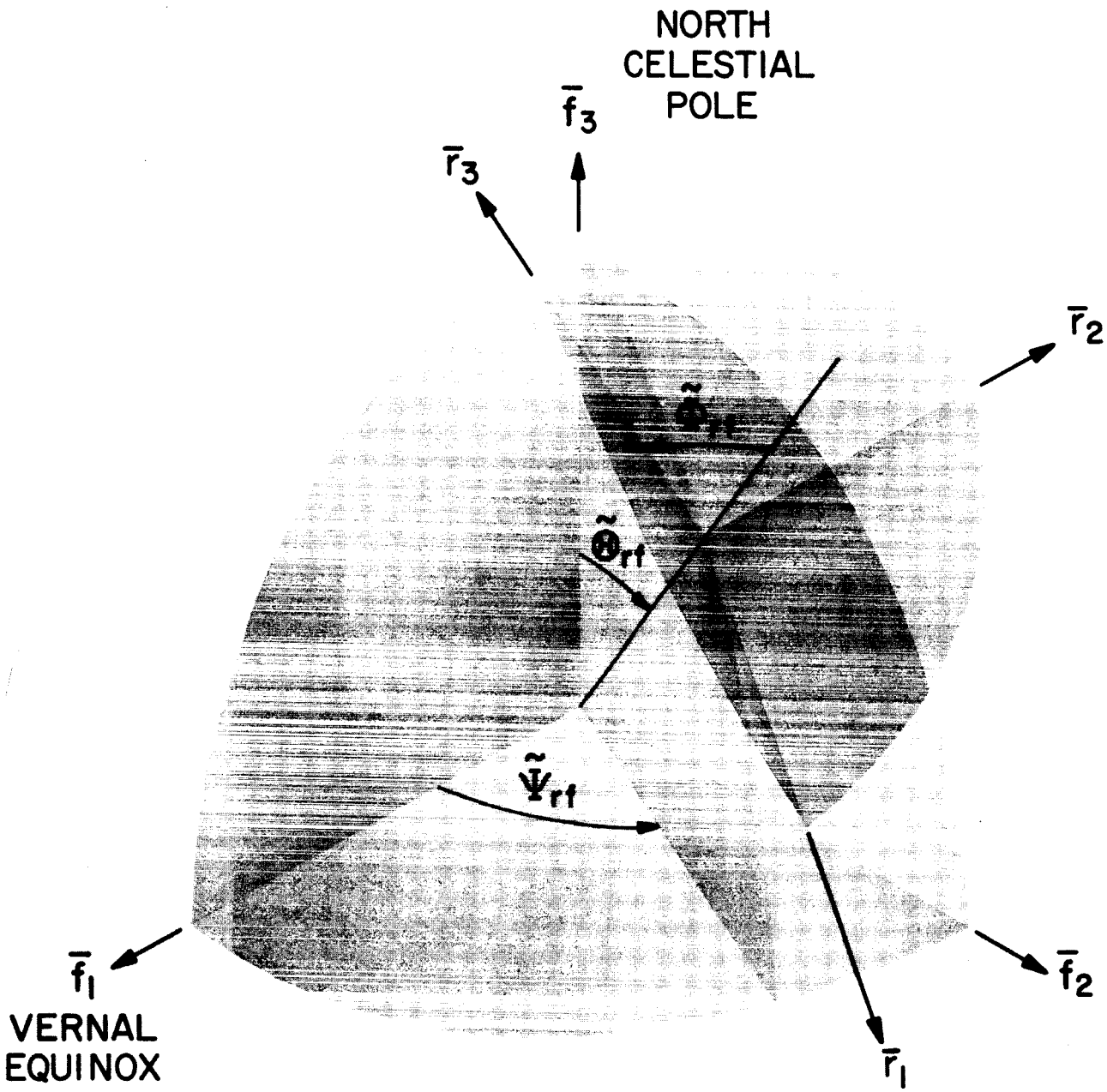

Figure 9.- Body reference frame with respect to inertially fixed frame.

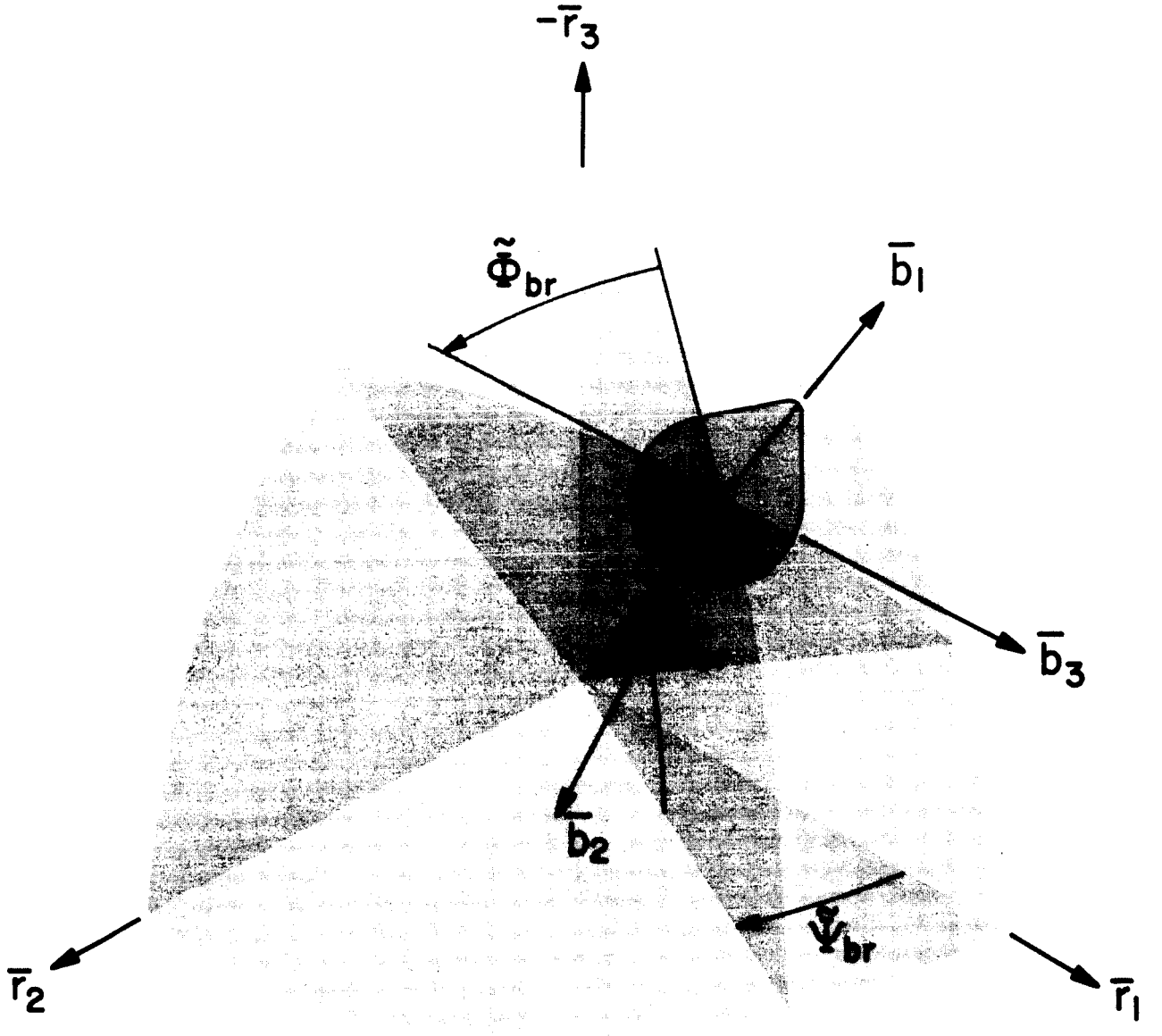

Figure 10.- Body frame with respect to body reference frame.

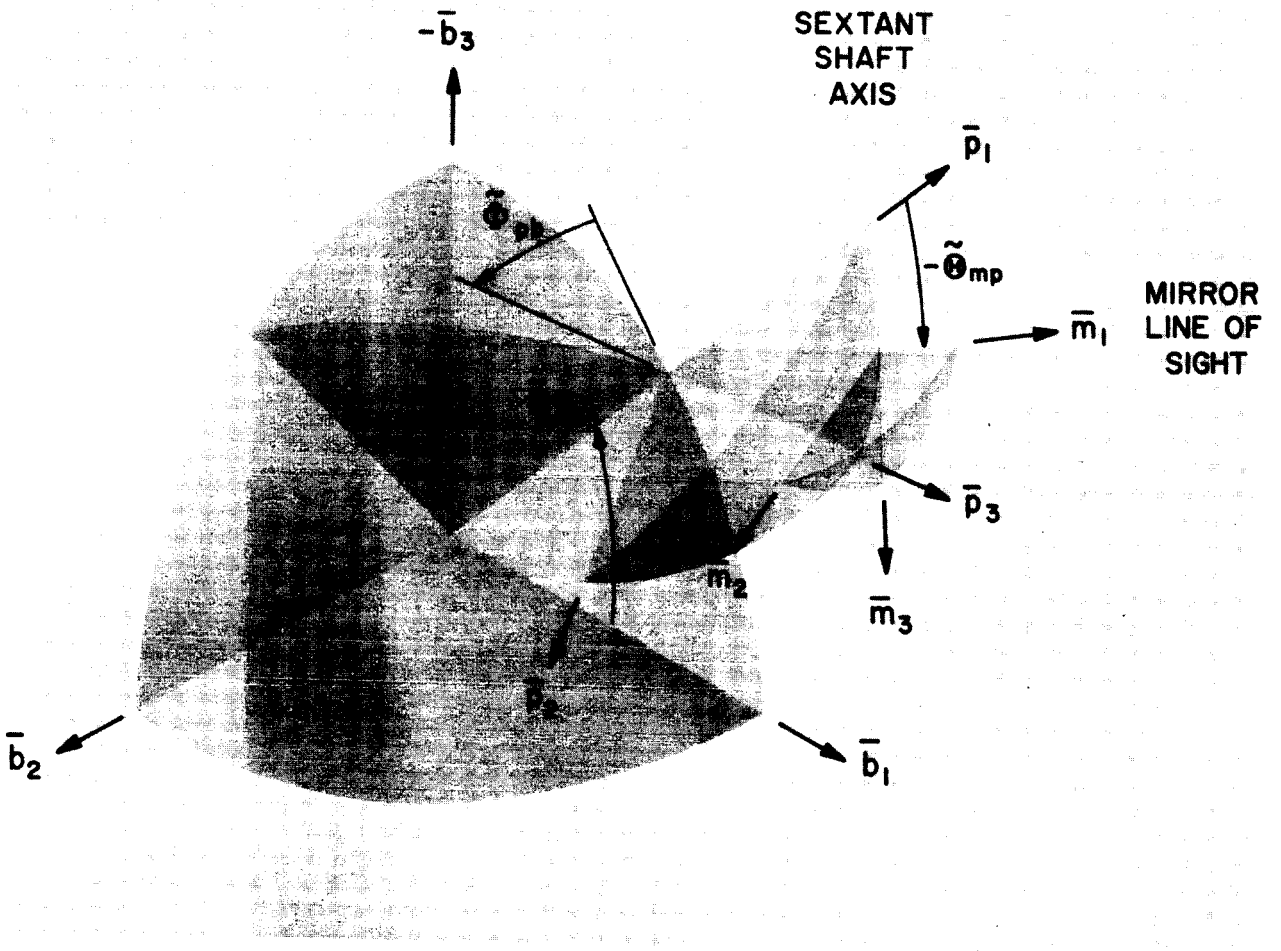

Figure 11.- Sextant mirror frame and sextant shaft frame with respect to body frame.

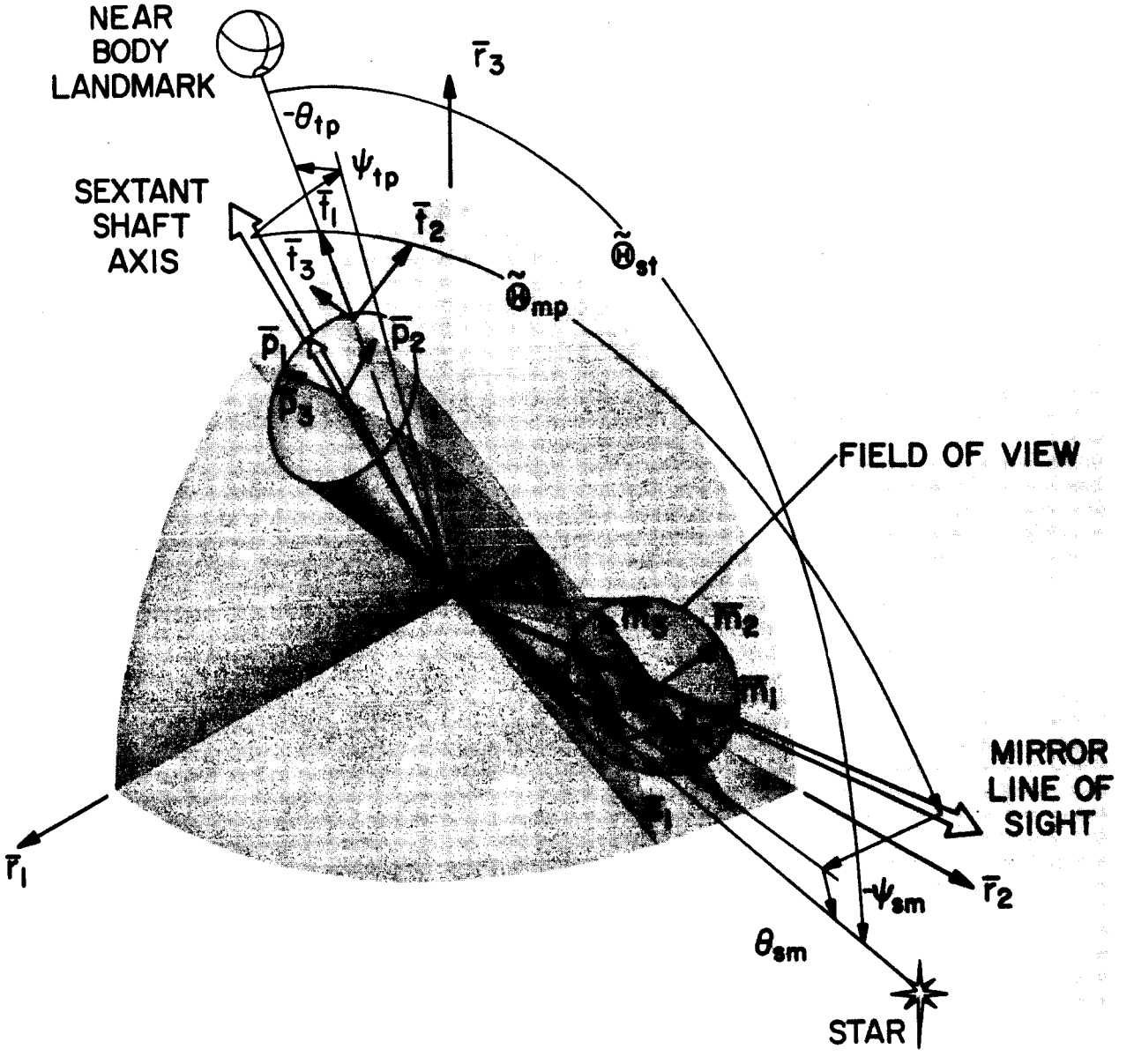

Figure 12.- True line of sight frames with respect to sextant mirror and shaft frames.

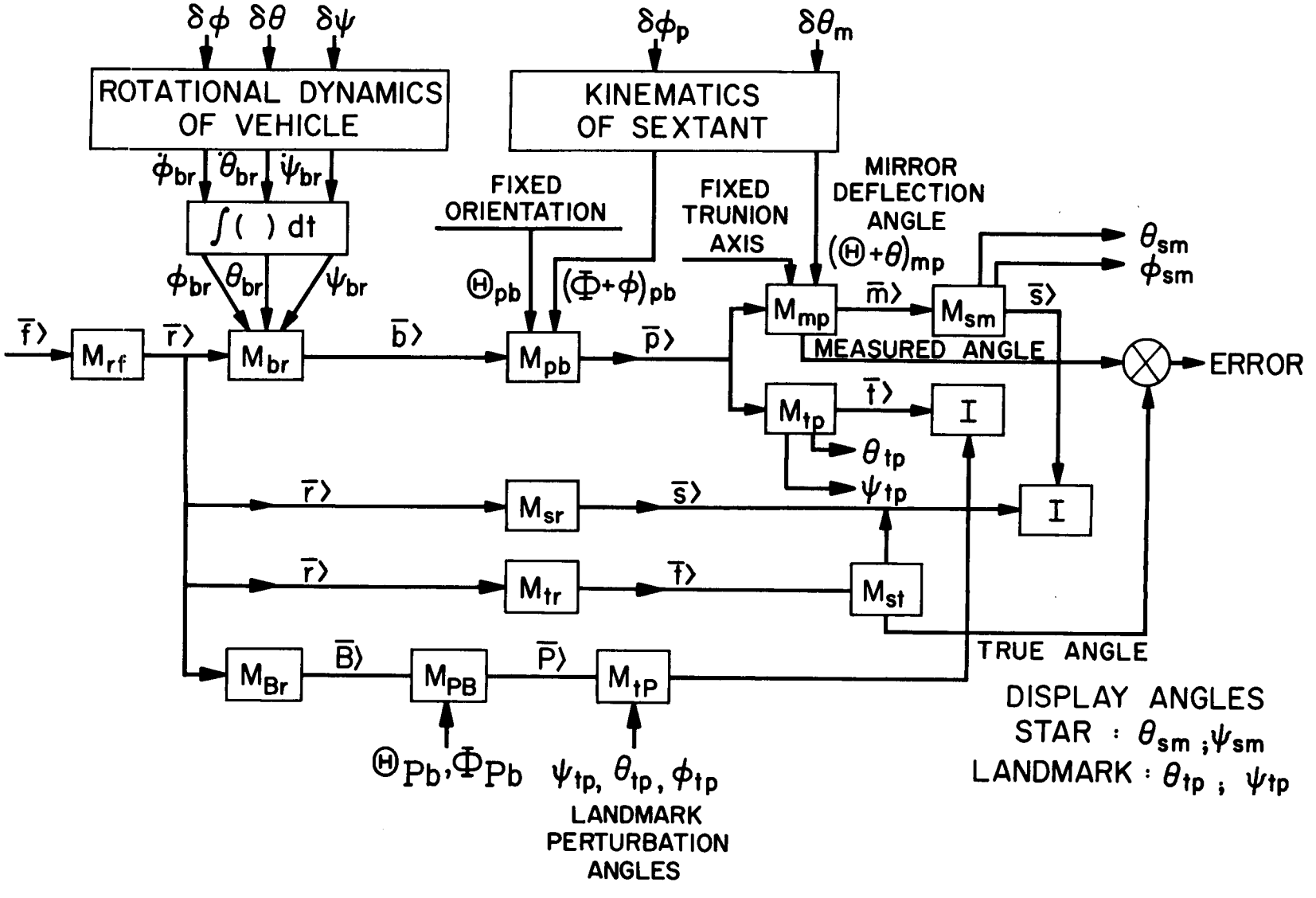

Figure 13.- Sextant simulation reference frame flow diagram.

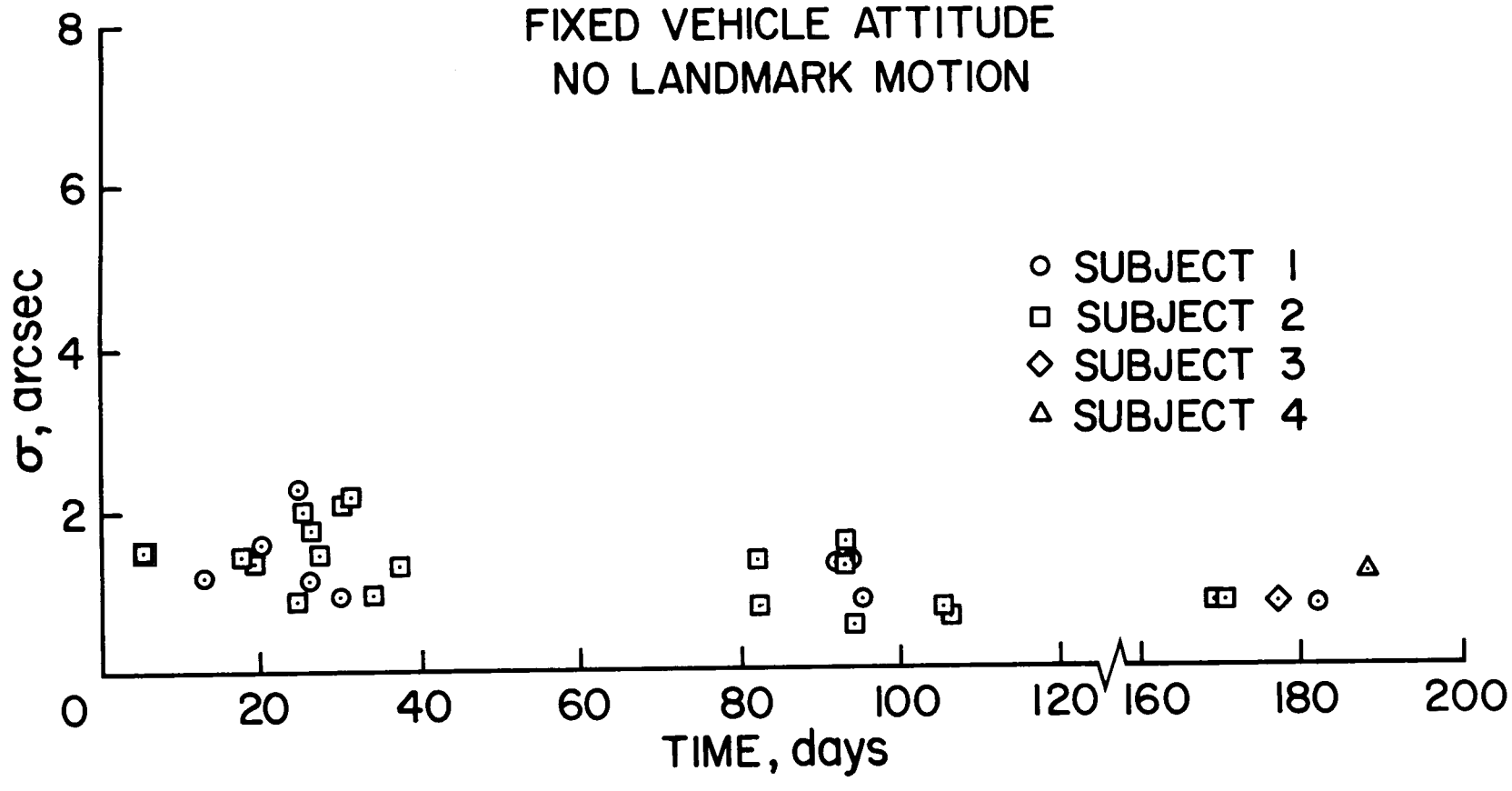

Figure 14.- Chronological base-line performance data.

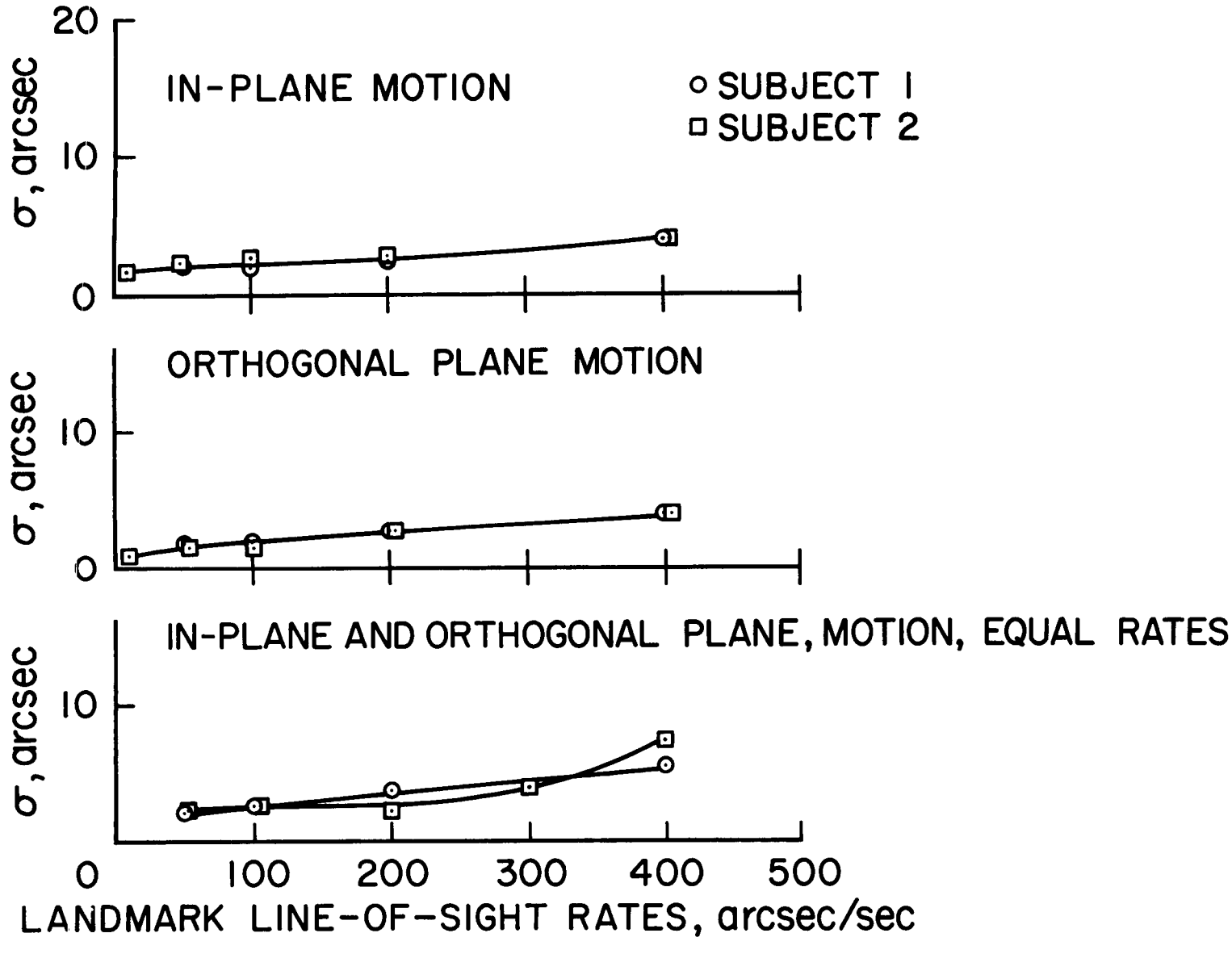

Figure 15.- Effect of landmark line-of-sight rates on accuracy with vehicle attitude controller active and no initial vehicle attitude rates.

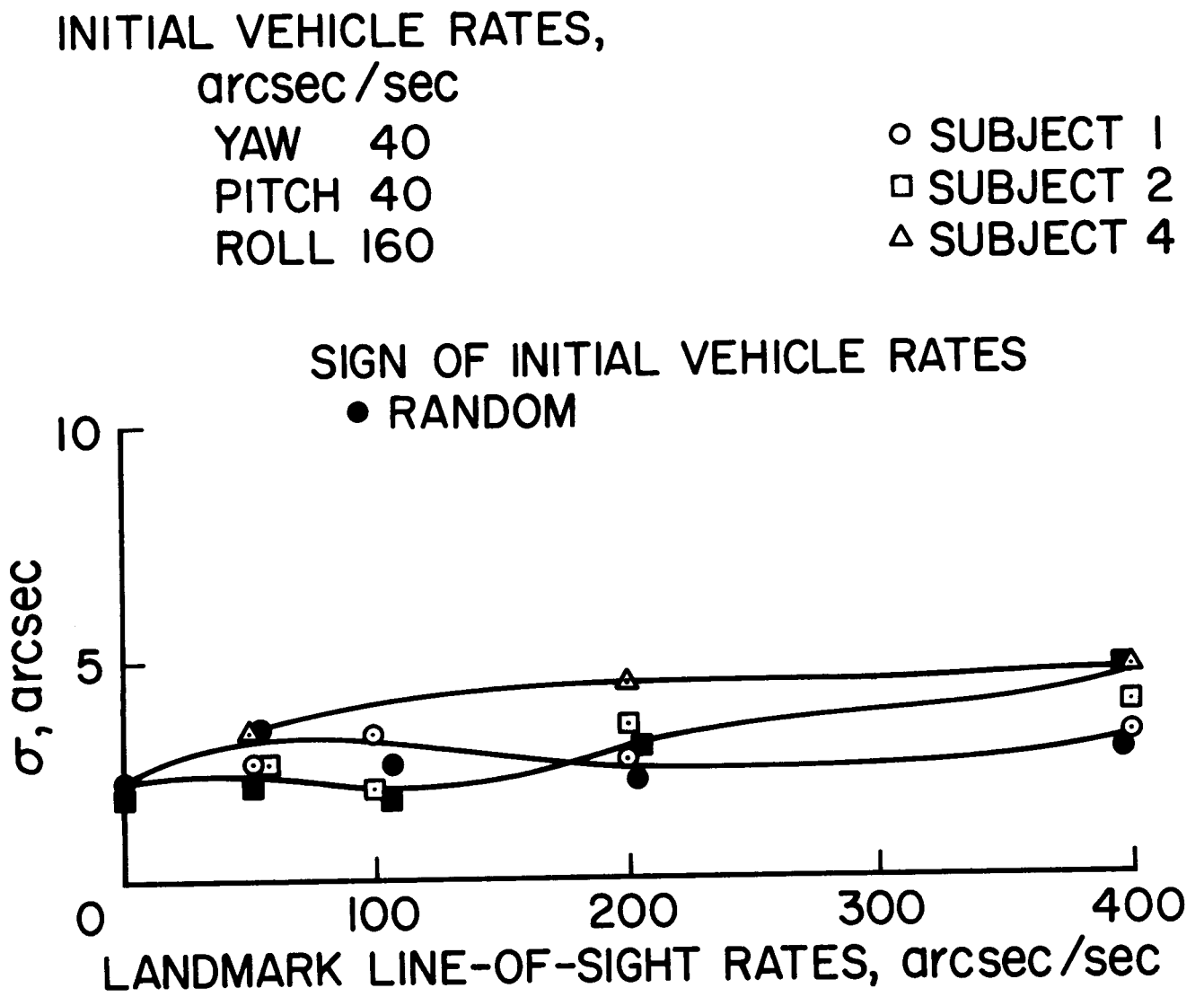

Figure 16.- Effect of combined landmark line-of-sight rates and initial vehicle attitude rates on sighting accuracy.

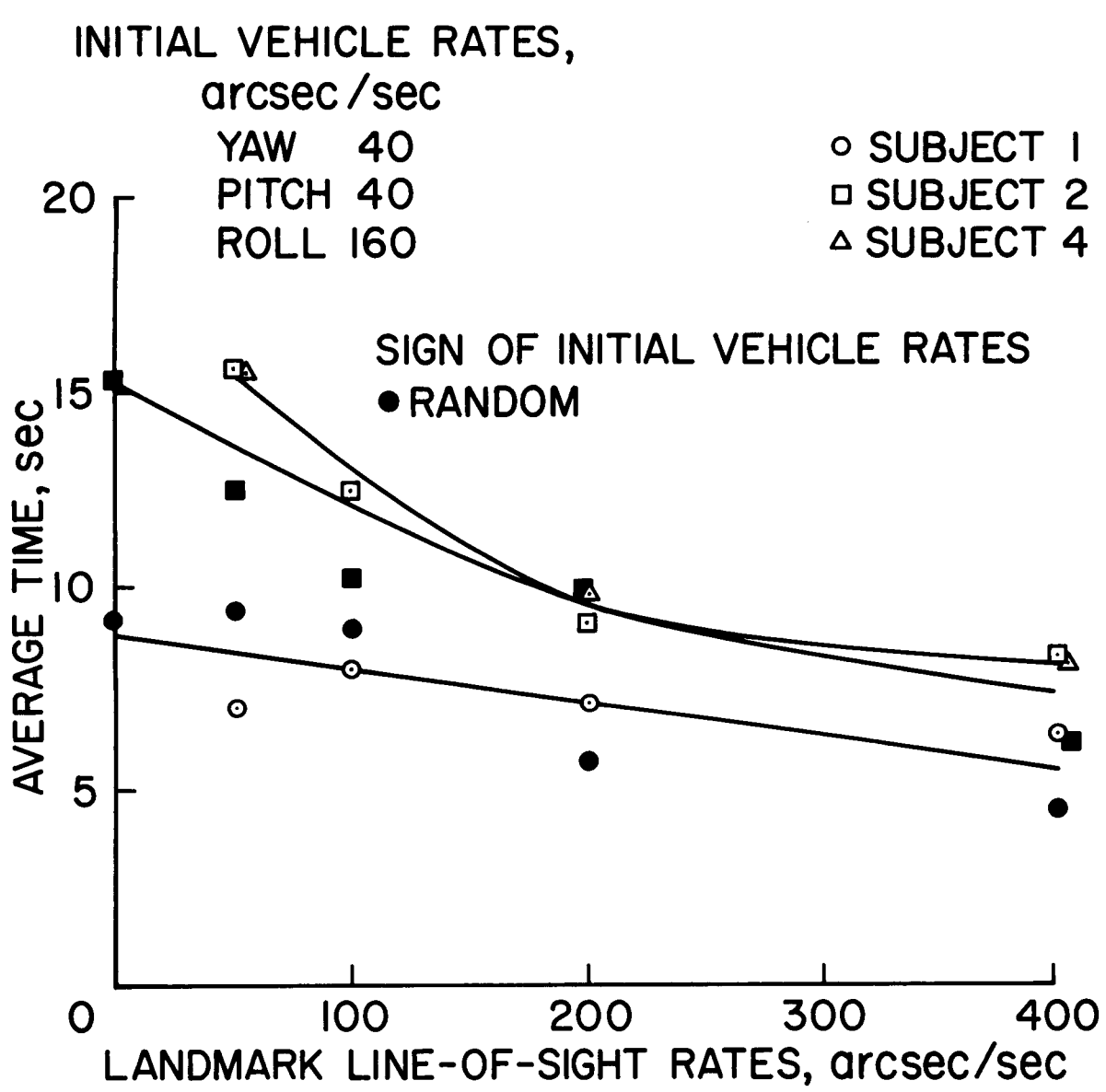

Figure 17.- Effect of combined landmark line-of-sight rates and initial vehicle attitude rates on average sighting time.

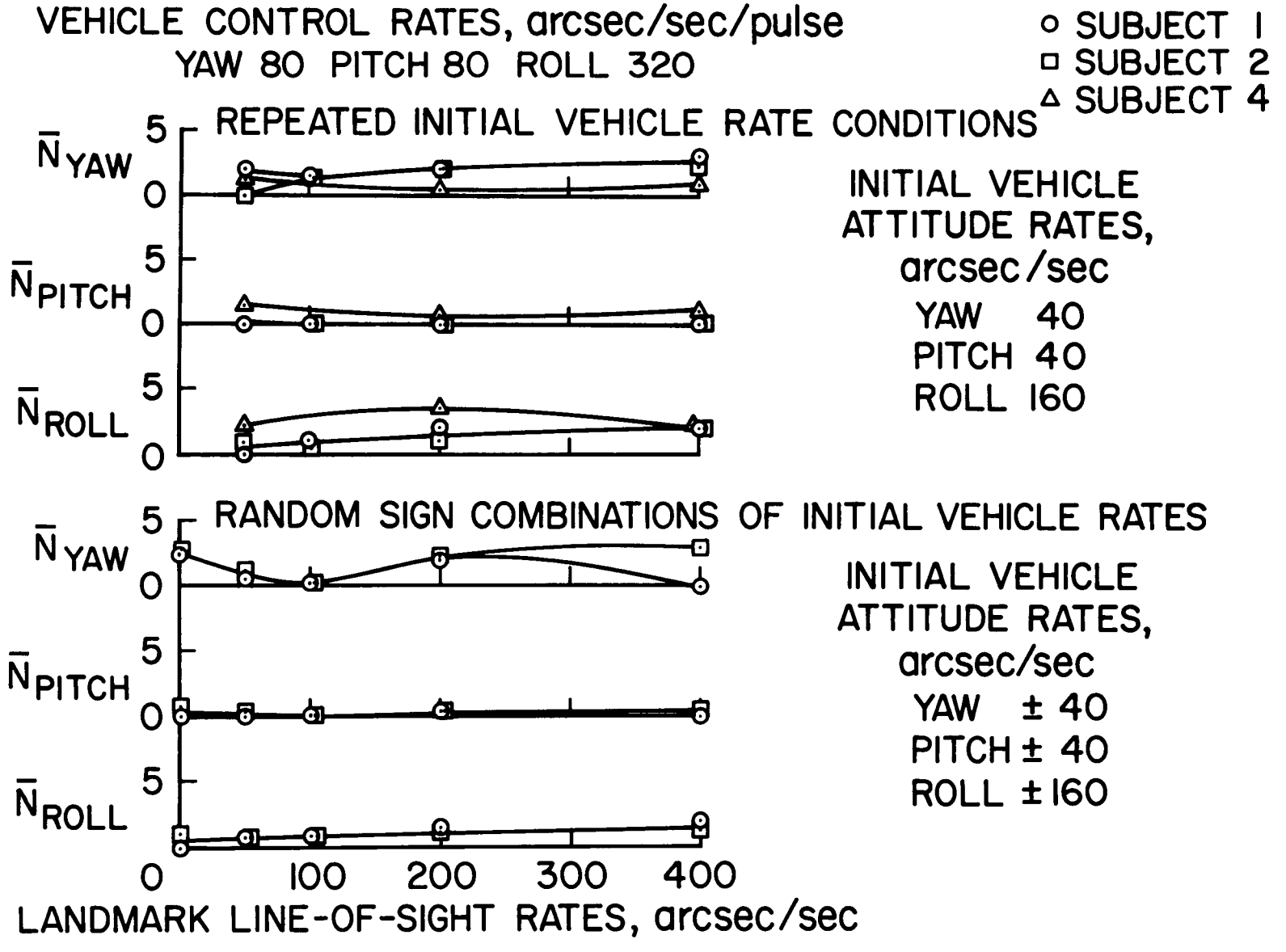

Figure 18.- Effect of combined landmark line-of-sight rates and initial vehicle attitude rates on average number of control pulses.

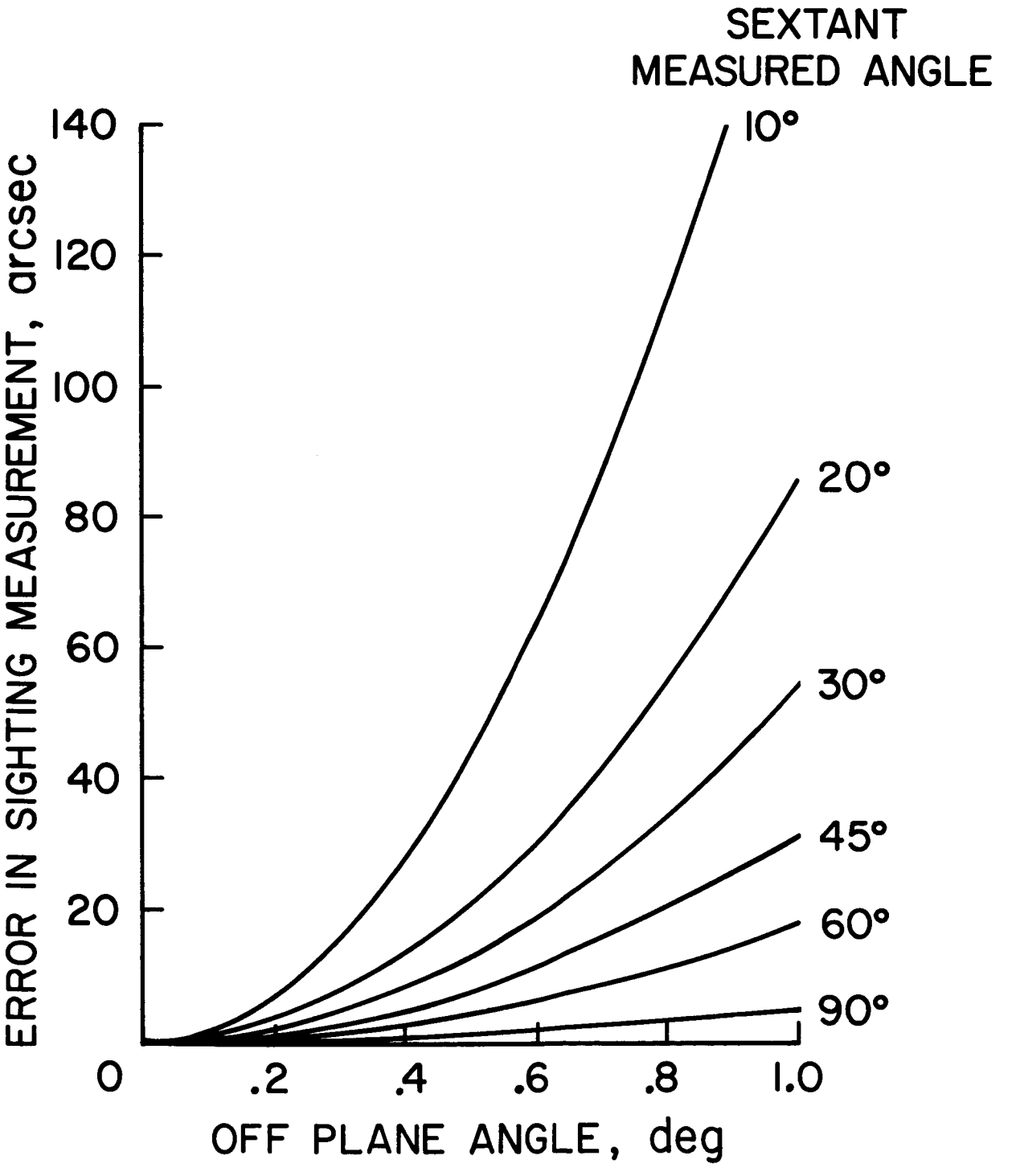

(a) Case I: Landmark on plane, star off plane.

Figure 19.- Sextant measurement error due to off plane sightings.

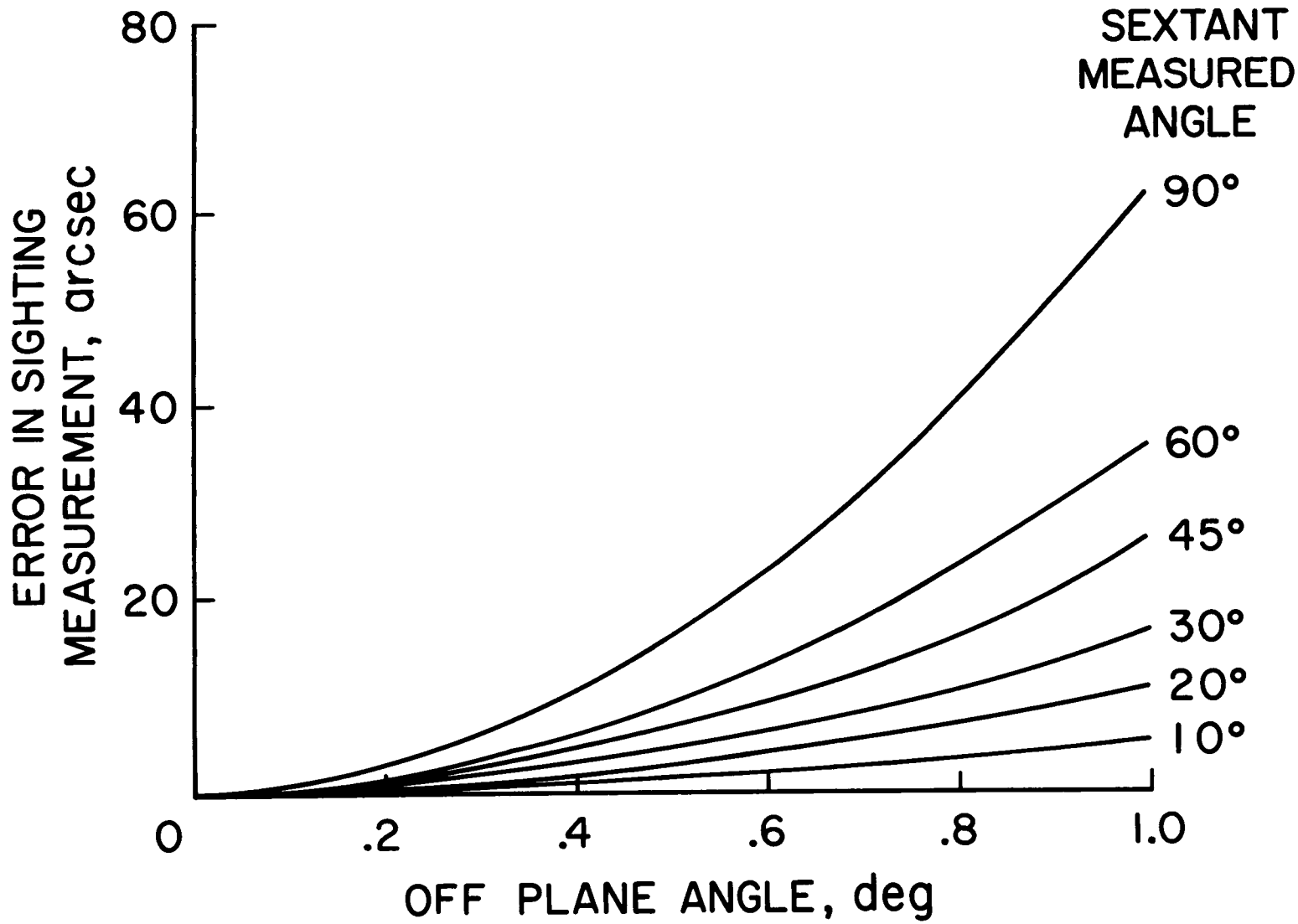

(b) Case II: Landmark and star superimposed off plane.

Figure 19.- Continued.

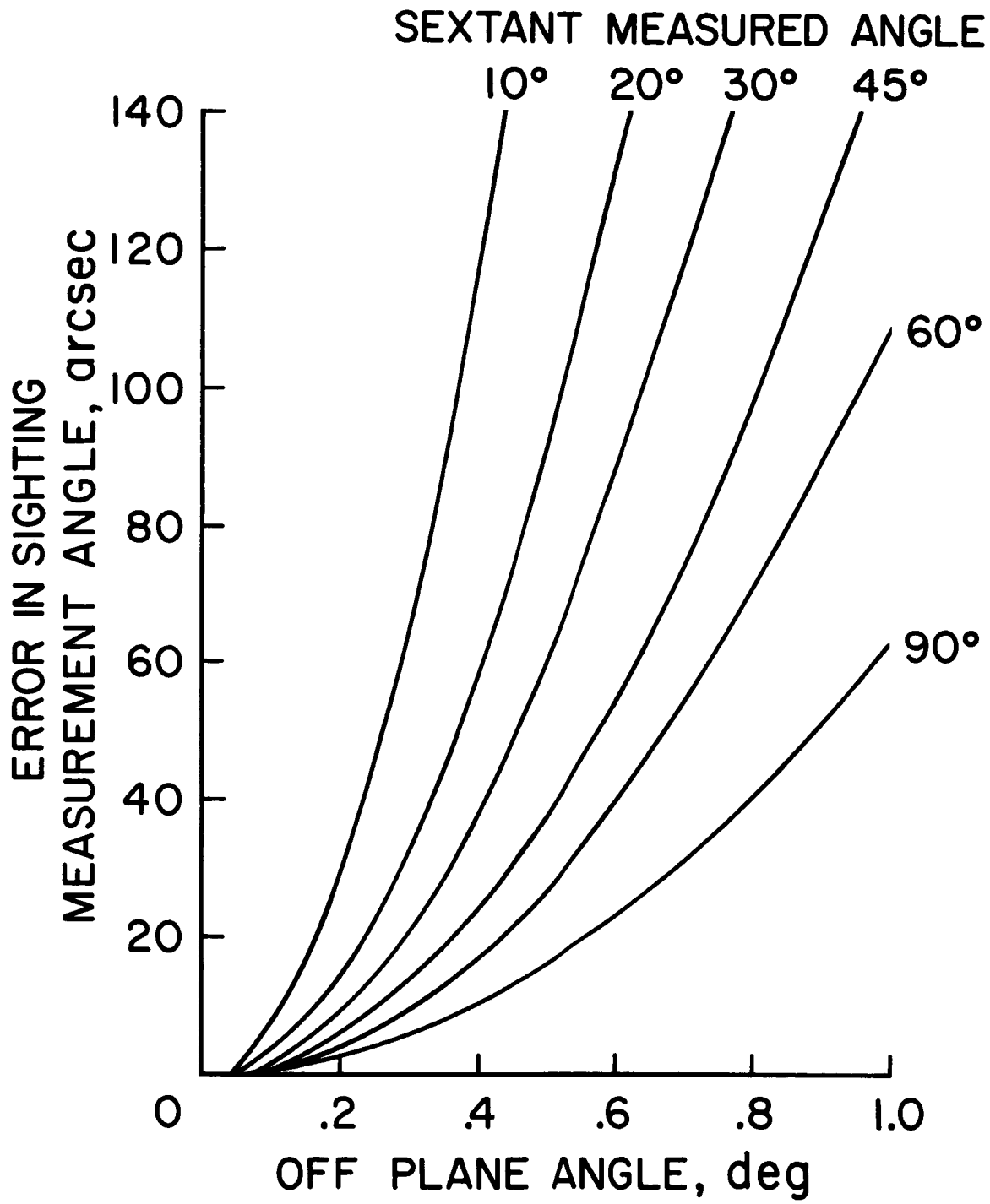

(c) Case III: Landmark and star on opposite sides of plane.

Figure 19.- Concluded.